Solid Earth

Open Access

EGU

Insights into the tectonic evolution of the Svecofennian orogeny based on in situ Lu–Hf dating of garnet and apatite from Olkiluoto, southwestern Finland

Jon Engström[1,2], **Kathryn Cutts**[1], **Stijn Glorie**[3], **Esa Heilimo**[4], **Ester M. Jolis**[1], and **Radoslaw M. Michallik**[1]

[1]Geological Survey of Finland, P.O. Box 96, 02151 Espoo, Finland
[2]Department of Geology and Mineralogy, Åbo Akademi University, Akatemiakatu 1, 20500 Turku, Finland
[3]Department of Earth Sciences, University of Adelaide, Adelaide, SA 5005, Australia
[4]Department of Geography and Geology, University of Turku, Akatemiakatu 1, 20500 Turku, Finland

Correspondence: Jon Engström (jon.engstrom@gtk.fi)

Abstract. The southern Finland granites and associated migmatitic rocks have a complex metamorphic history, being affected by multiple events during the ca. 1.88–1.79 Ga Svecofennian orogeny. In this study, the prolonged tectonic evolution of migmatites and associated rocks in southwestern Finland has been investigated using the new in situ Lu–Hf method. Results reveal detailed temporal constraints for the tectonic evolution that can be linked to major events in adjacent tectonic blocks in both Finland and Sweden during the Svecofennian orogeny. The metamorphic peak at the Olkiluoto site occurred at 1829 ± 19 Ma based on in situ Lu–Hf dating of garnet. The pressure–temperature (P–T) path for the rocks indicates a prograde evolution, with peak P–T conditions of 3–5 kbar and approximately 700 °C. Younger ages of ca. 1780 Ma obtained using both Lu–Hf and U–Pb systems in apatite inclusions in garnet indicate rapid cooling at 1780 Ma. Based on the metamorphic constraints and obtained ages, we link the Olkiluoto site to the Häme orogenic belt in southern Finland and also support the proposed thermal–tectonic connection with the Ljusdal lithotectonic unit in central Sweden.

1 Introduction

The tectonic evolution and the metamorphic record from the latter parts of Svecofennian orogeny have in the past been inferred to be similar in southern Finland and central Sweden (Hietanen, 1975; Korja and Heikkinen, 2005; Högdahl and Bergman, 2020; Engström et al., 2022). However, the coupling between these regions has been challenging to establish due to the prolonged tectonic evolution and the polymetamorphic nature of the Palaeoproterozoic bedrock, which often obscures the detailed pressure–temperature–time (P–T–t) record for these rocks. Thus, novel geochronological techniques, particularly in situ Lu–Hf geochronology focusing on key metamorphic minerals like garnet and apatite, are indispensable for accurately delineating and investigating these ancient polymetamorphic terranes, especially since they retain information of past metamorphism in rocks that have seen multiple tectonic events that is typical of rocks in ancient orogenies (Tamblyn et al., 2022). Dating garnet, coupled with conventional geochronological techniques such as U–Pb geochronology on accessory zircons and monazite, is beneficial because garnet as a metamorphic mineral clearly represents the metamorphic age of the rock and can also provide information about the pressure–temperature (P–T) evolution of the rock (Brown et al., 2022; Tamblyn et al., 2022; Simpson et al., 2023). Using garnet and apatite Lu–Hf geochronology in tandem is a powerful tool for understanding the thermal evolution of metamorphic rocks due to the difference in closure temperature of the Lu–Hf system in garnet (> 800 °C; Smit et al., 2024) and apatite (670–730 °C; Glorie et al., 2024a), this is essential information for understanding polymetamorphic rocks.

This study focuses on resolving the tectonic evolution in the Olkiluoto study area, which was affected by two meta-

morphic events during the Palaeoproterozoic Svecofennian orogeny (Tuisku and Kärki, 2010; Saukko et al., 2020). The Palaeoproterozoic bedrock of southern Finland consists to a large extent of granitoids and migmatites (e.g. Nironen, 2017). Based on lithological, geochemical, and geochronological data, the Svecofennian crustal domain in Finland is divided into two major lithotectonic units: the Western Finland Subprovince (WFS) and the Southern Finland Subprovince (SFS) (Fig. 1; Korsman et al., 1997; Väisänen et al., 2002; Lahtinen et al., 2005; Nironen, 2017). The Svecofennian Province of Finland is separated from the Ljusdal lithotectonic unit in central Sweden (Högdahl and Bergman, 2020) by the Gulf of Bothnia. Despite this geographical separation, both regions show similar characteristics in terms of the rock types and structures (Fig. 1). These similar characteristics are comparable magmatic activity and similar structural evolution coupled with the same style and timing of metamorphism (e.g. Kähkönen, 2005; Nironen, 2005; Bergman et al., 2008; Väisänen et al., 2012; Högdahl and Bergman, 2020).

The Olkiluoto site is the location for the Finnish deep geological repository for spent nuclear fuel, and this study is part of the geological site characterization. Our investigation provides new insights into the tectonic history of the Olkiluoto site and southwestern Finland during the Palaeoproterozoic Svecofennian orogeny (Fig. 1). The tectonic evolution has been defined through the analysis of garnet, a key mineral that serves as a reliable indicator of metamorphic conditions and thermal history within the crust. We have used the recently developed in situ Lu–Hf geochronology employing the use of laser ablation inductively coupled plasma tandem-quadrupole mass spectrometry (LA-ICP-Q-MS/MS) (Brown et al., 2022; Simpson et al., 2021, 2023) to demonstrate that garnet and also apatite in felsic, migmatitic, and tonalitic–granitic–granodioritic (TGG) intrusive rocks show metamorphism with one distinct metamorphic event and possibly an earlier event. Even though the Olkiluoto investigation area is small, the results of this study can be connected to a more regional context regarding the tectonic framework in southern Finland. The Lu–Hf geochronology from the Olkiluoto site, combined with pressure–temperature modelling, provides new insight into how metamorphic processes and tectonic events were interconnected in southern Finland. This knowledge is important for establishing connections with the Ljusdal lithotectonic unit in central Sweden. Recent studies by Engström et al. (2022), Lahtinen et al. (2023), and Luth et al. (2024) infer that the coupling of the Olkiluoto area to central Sweden is plausible. However, more constraints and detailed research is required from adjacent areas in southwestern Finland and central Sweden to define the tectonic and metamorphic evolution and the coupling between these two areas.

2 Geological setting of the study area

2.1 Tectonic framework

The Palaeoproterozoic Svecofennian orogeny and its corresponding crustal province were first introduced in the classic review by Gaál and Gorbatschev (1987) (Fig. 1). Since then, several tectonic models have been presented for the evolution of the accretionary orogen (e.g. Nironen, 1997, Lahtinen et al., 2005, Lahtinen et al., 2023). The orogeny initiated from 1.92 to 1.87 Ga (Nironen, 2017; Heilimo et al., 2023) with a collisional stage during which several volcanic arc complexes or microcontinents laterally accreted onto the margin of the Archean Karelia craton (e.g. Lahtinen et al., 2005). The Svecofennian orogeny is characterized by two main high-T and low-P type metamorphic events. The first event occurred at 1.88–1.87 Ga, reaching upper amphibolite facies, and can be detected throughout the Finnish Svecofennian (Korsman et al., 1999; Nironen, 2017). The convergence stage included several thrust sheets that developed within a W–SW to E–NE compressional environment in southern Finland (Nironen, 2017; Torvela and Kurhila, 2020). The Western Finland Subprovince (WFS) was subjected to moderate crustal thickening and the widespread development of granites and associated migmatites related to either channelized flow or in situ melting of metasedimentary rocks, with peak metamorphism occurring at 1.88–1.87 Ga (Mäkitie et al., 2012; Chopin et al., 2020). The subsequent tectonic phases included minor crustal extension, followed by the resumption of orogenic convergence that resumed at ca. 1.84 Ga, and especially in southern Finland this initiated a younger metamorphic event that formed granites and associated migmatites (Lahtinen et al., 2005; Torvela et al., 2008; Torvela and Kurhila, 2020; Kara et al., 2021). The younger metamorphic event involved high-T metamorphism to granulite facies in large areas of southernmost Finland and was associated with emplacement of granites together with anatectic melting, resulting in the formation of migmatites and pegmatites during the late stages of the Svecofennian orogeny (Korsman et al., 1999; Väisänen and Hölttä, 1999; Väisänen et al., 2002; Skyttä and Mänttäri, 2008). This transpressional deformation phase was characterized by intensive folding and shear zone development (Ehlers et al., 1993; Torvela and Kurhila, 2020; Väisänen et al., 2002; Väisänen and Skyttä, 2007).

The Svecofennian rocks within the Ljusdal lithotectonic unit, central Sweden, were intruded by the Ljusdal Batholith at ca. 1.86–1.84 Ga (Högdahl et al., 2008) and were affected by polyphase, ductile deformation that was coupled to two episodes of high-grade, low-pressure metamorphism during the Svecofennian orogeny that is dated at ca. 1.85 and 1.83–1.82 Ga, with prolonged crustal heating continuing to at least 1.80 Ga (Högdahl et al., 2008; Högdahl and Bergman, 2020, see Fig. 1). The latter metamorphic events in central Sweden (1.83–1.82 Ga) and southern Finland (1.84–1.80 Ga) show
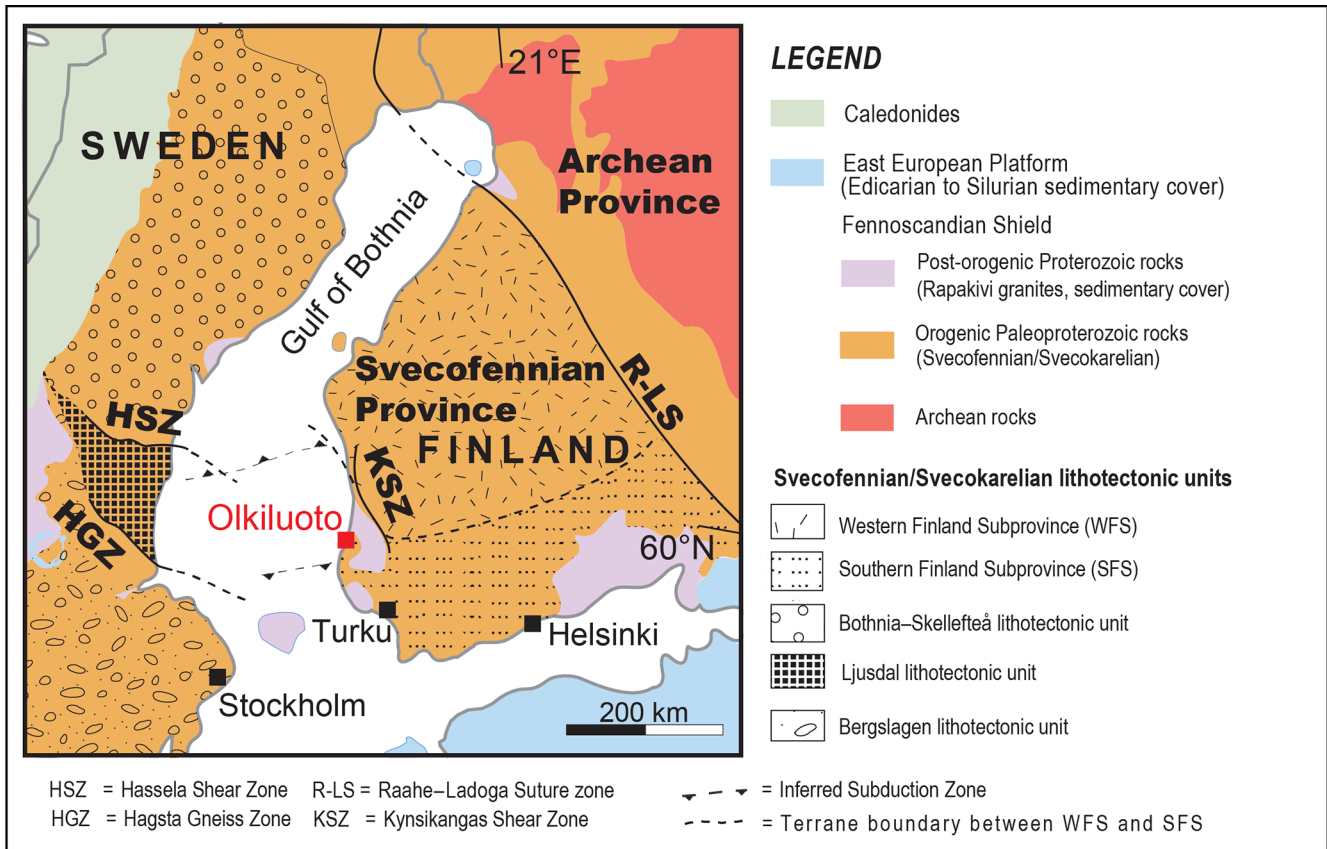
Figure 1. Synthetic geological map of the Fennoscandian shield. Olkiluoto is indicated with a red square. Map modified from Koistinen et al. (2001), Korja and Heikkinen (2005), Nironen (2017), and Stephens (2020).

especially similar tectonic evolution and metamorphic signatures, and thus a connection between the Olkiluoto site and the Ljusdal lithotectonic unit in central Sweden can be deduced (Högdahl et al., 2008; Engström et al., 2022).

2.2 Geology of the Olkiluoto area

According to Engström et al. (2022), the Olkiluoto site experienced a tectonic evolution where ductile deformation took place in several steps, coinciding with the formation of migmatites and leucosomes under high-T conditions in the Palaeoproterozoic crust. Thus, the bedrock at Olkiluoto island consists of Palaeoproterozoic, mostly intrusive and supracrustal (meta-pelites, meta-arenites and meta-volcanic) rocks and is situated in the westernmost part of the Southern Finland Subprovince (SFS) (Figs. 1 and 2). The felsic, tonalitic-granitic-granodioritic (TGG) intrusive rocks are migmatized with small, injected veins of pegmatitic–granitic (PGR) leucosome. Since this TGG intrusive rock is less deformed and altered by the subsequent polyphase ductile deformation events compared to the metapelitic supracrustal migmatitic rocks (Engström et al., 2022), it is well suited for our study on the metamorphic evolution in Olkiluoto. The whole bedrock at the site is also intruded by diabase dykes,

likely of Mesoproterozoic age (Mänttäri et al., 2006). The migmatites in Olkiluoto are divided into two main groups: vein- and dyke-structured metatexites (VGN in Fig. 2) and nebulitic diatexites (DGN in Fig. 2), which can be further subdivided into several subtypes on the basis of their migmatite structures (Kärki, 2015). Metatexitic migmatites dominate the northwestern part of the island, whereas diatexites are abundant in the southeastern part of the island (Fig. 2).

Earlier studies indicate that two distinct metamorphic events occurred in Olkiluoto (Tuisku and Kärki, 2010; Saukko et al., 2020; Engström et al., 2022), with the metamorphic conditions of the first event (M1, older) estimated to have a peak pressure of approximately 6 kbar but no information on temperature. This M1 event was interpreted based on some samples giving a higher estimated peak pressure than the average metamorphic grade (3–4 kbar), and this event was also interpreted to be early and connected to magmatic processes and emplacement of the protolith of TGG rocks (Tuisku and Kärki, 2010). Even though the earlier metamorphic studies lack temperature information, the study by Saukko et al. (2020) concluded that two generations of migmatitic events with leucosome production did occur
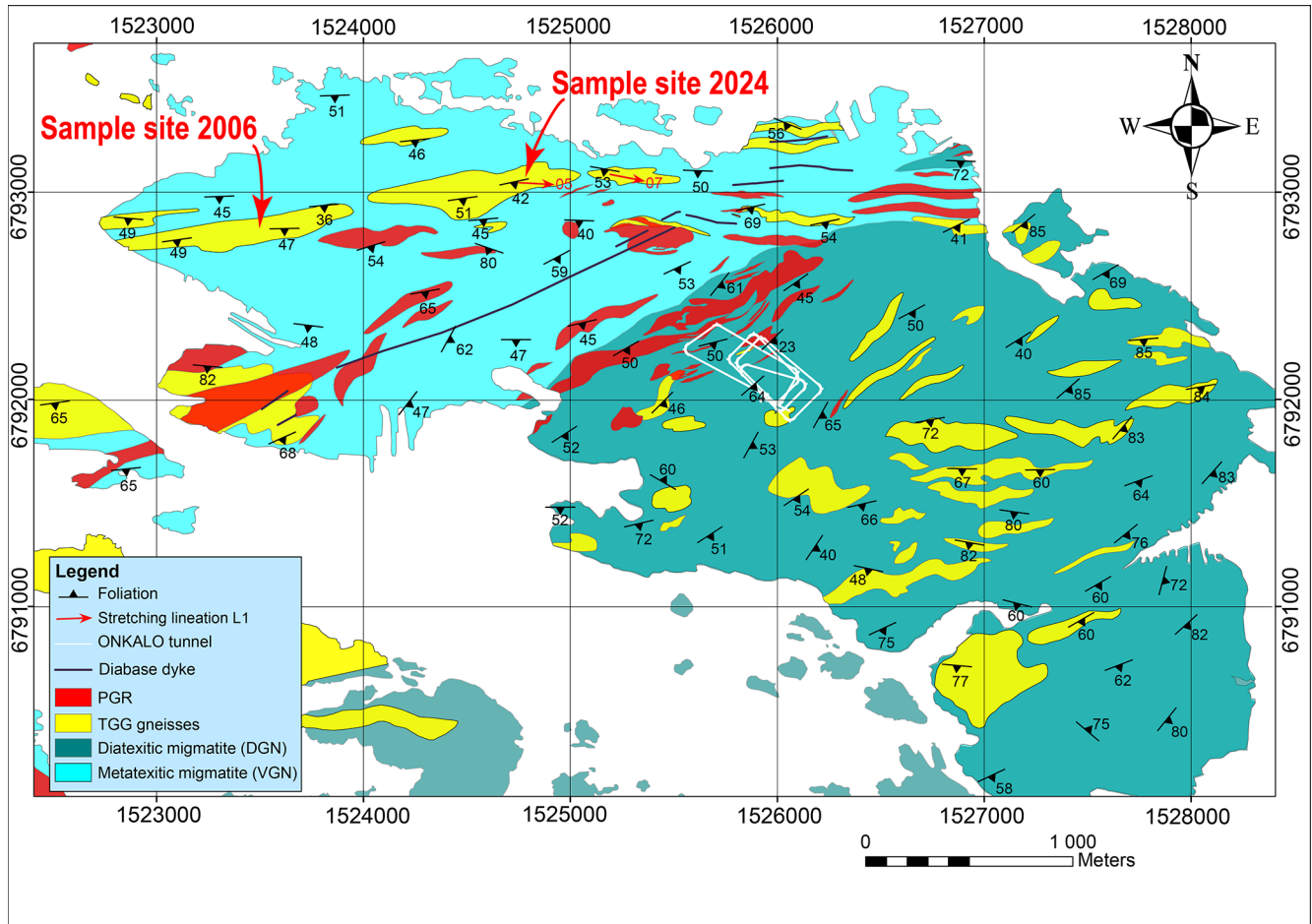
Figure 2. Geological map of Olkiluoto (modified from Aaltonen et al., 2016, and Engström et al., 2022). The locations of the investigated outcrops in 2024 and 2006 are also indicated. Coordinate system in the map is the Finnish Projected KKJ Zone 1.

in Olkiluoto. The mineral assemblages of the second metamorphic peak (M2, younger) are indicative of upper amphibolite facies, stable at 660–700 °C and 3.7–4.2 kbar (Tuisku and Kärki, 2010). The timing of these tectono-metamorphic events are constrained using tectonic events and metamorphic U–Pb zircon ages at ca. 1.87–1.84 and 1.82–1.78 Ga, respectively (Engström et al., 2022). The pressure difference of approximately 2 kbar between the two metamorphic stages indicates either an erosion phase between the metamorphic phases or a significant crustal uplift, but another possibility is an interplay between both processes. The M2 metamorphic event is characterized by injected granitic and pegmatitic leucosome veins and dykes that are crosscutting the earlier generated foliation (Engström et al., 2022).

3 Methodology

3.1 Outcrop description

This study includes whole-rock geochemistry of the different lithological units at the site coupled with a detailed outcrop study of the TGG intrusive rock representing the protolith for the metamorphic rock in the M1 metamorphic phase in Olkiluoto (Engström et al., 2022). Detailed structural geological mapping of the TGG outcrop was performed to guide the sampling for garnets (see Fig. 2, sample site 2024). From the studied outcrop (see Fig. 2, sample site 2024), two rock samples (approx. 50 cm × 10 cm × 8 cm) were collected for further investigation (Fig. 3). The samples MM30 (predominantly small garnets, Fig. 3a–b) and MM31 (predominantly big garnets, Fig. 3c–d) were chosen carefully during the mapping to have a structural control since the big garnets in MM31 were observed with the leucosome on the outcrop. The samples are separated by 3–4 m and during detailed investigation are shown to be compositionally similar, with both containing large subhedral garnet crystals up to 3–5 cm
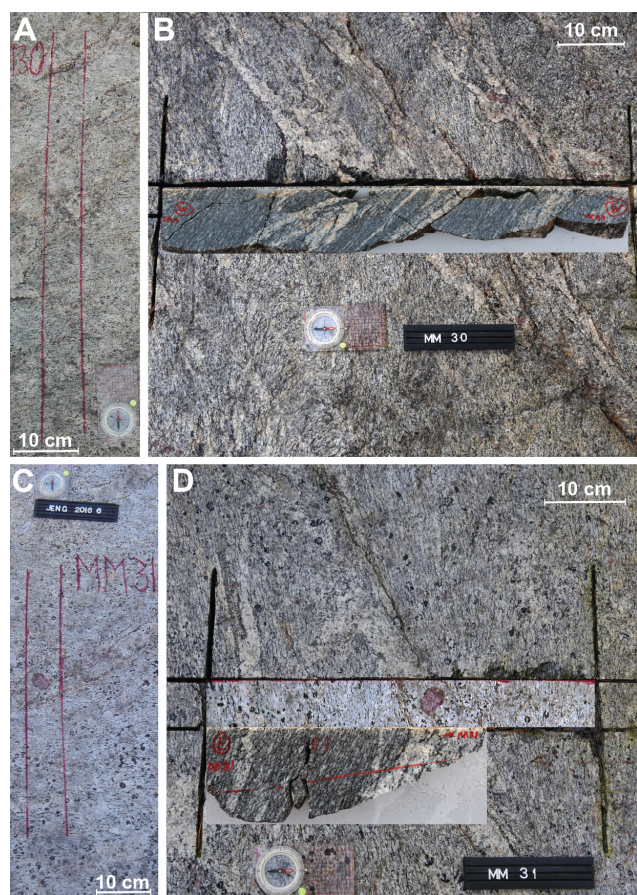
Figure 3. The TGG outcrop indicating the sawed-out rock sample areas. Sample area MM30, with a view from the top (**a**) and with a cut-out (**b**). Sample area MM31, with view a from the top (**c**) and with a cut-out (**d**).

in size in leucosomes and small (up to 0.3–0.7 cm in size) anhedral garnet crystals within the mesosome. Garnet grains were selected from these samples for microanalytical and petrochronological analysis, such as thin sections and micro-XRF images. Both large (MM31) and small (MM30) garnets were targeted for Lu–Hf analysis. Apatite inclusions in the large garnet (MM31) were targeted for Lu–Hf and U–Pb analysis.

3.2 Sample description

The TGG bedrock in the northwestern part of the Olkiluoto site was chosen for this study, since it has been least affected by the different polyphase ductile deformation events, especially concerning later folding and migmatization events. The rocks are pale grey in colour and contain a compositional banding with a prominent stretching lineation of feldspars. Garnet occurs as small grains scattered in the mesosome (sample MM30) and as large grains that occur within leucosomes (sample MM31). Both types of garnet were targeted in this study to determine if they grew during single or mul-

tiple phases of metamorphism. The small garnet grains (up to 0.7 cm, MM30) (Fig. 3a–b) were removed from one of the collected samples by slicing it with a small saw and then picking out the small grains where they were observed. Three small grains were then mounted in a single 2.5 cm epoxy mount. The large garnet grain was embedded in the leucosome (ca. 5 cm) of sample MM31 (Fig. 3c–d), was removed by sawing, and was then cut in half in order to fit the 2.5 cm epoxy mount. The mineralogy of the rock samples consists of quartz, K-feldspar, plagioclase, biotite, and garnet, with accessory apatite and cordierite, which often exhibit pinite alteration (Fig. 4). These are coarse-grained samples, with K-feldspar grains up to 1 cm and plagioclase and quartz of up to 0.5 cm (Fig. 4b–c). The grain size in the leucosome is larger, with K-feldspar, quartz, and garnet up to several centimetres in size. Garnet grains in both the mesosome and leucosomes have cores rich in quartz inclusions and often define a symplectitic-like texture (Fig. 4d). Rarely, biotite is also observed in garnet cores. Apatite inclusions commonly occur on the outer edge of the core domain and in the rims (Fig. 5). Garnet rims are generally poor in terms of inclusions, but where inclusions occur they are large and usually consist of quartz, apatite, biotite, or K-feldspar. Garnet grains are subhedral with irregular grain boundaries, often with embayments (Fig. 4d). The mesosome foliation is defined by biotite, which forms elongate grains up to several millimetres in size. Biotite is generally also slightly coarser in the leucosomes, and the foliation is not as well defined, with biotite grains often wrapping around large garnet grains. In both the mesosome and the leucosome, biotite grains are subhedral, often having scalloped grain edges. K-feldspar, quartz, and plagioclase all have irregular grain boundaries with scalloped edges; occur as rounded inclusions within each other; and form thin, film-like segregations (Fig. 4b–d). Larger grains are often elongate and oriented parallel to the foliation of the sample. Apatite is a common accessory mineral in the mesosome of the sample, and often it occurs as clumps of grains adjacent to large garnet grains but also as isolated grains with biotite or on feldspar and quartz grain boundaries.

3.3 Whole-rock geochemistry

All the sample preparation and analytical work for the whole-rock chemical samples was carried out at the SGS Minerals Services laboratory, Canada (Kärki and Paulamäki, 2006). Rock hand specimens (0.5–2 kg) were crushed by a magnesium steel jaw crusher and then pulverized in a carbon steel bowl. The analyses were done using an X-ray fluorescence (XRF) analyser, a neutron activation analyser (NAA), an inductively coupled plasma atomic emission analyser (ICP), an inductively coupled plasma mass spectrometer (ICP-MS), a sulfur and carbon analyser (LECO), and ion-specific electrodes (ISEs). The whole-rock sample for *P-T* modelling, MM30A (Table S1), was prepared at the university laboratories at Geohouse, Turku. A 1 kg sample was crushed
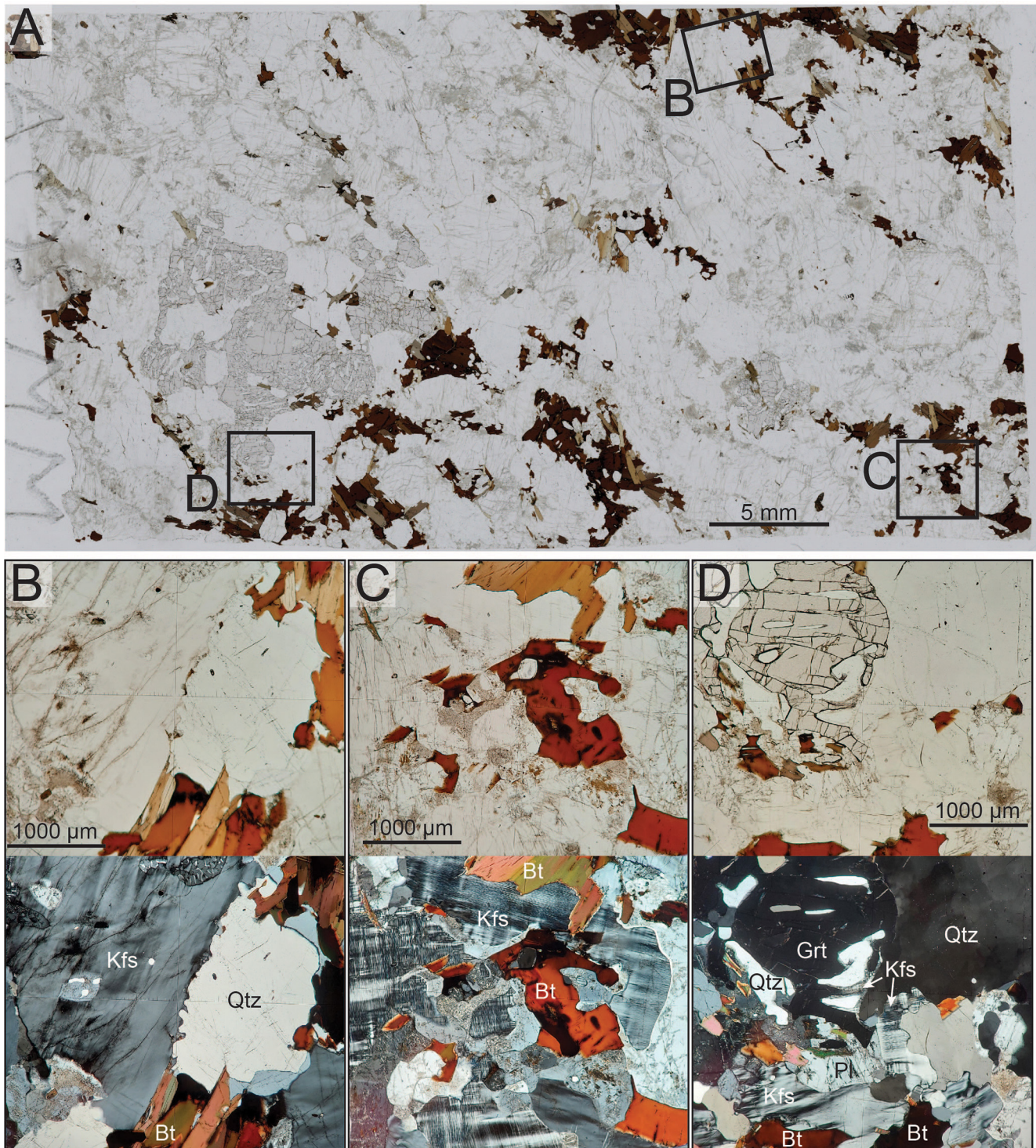
Figure 4. Sample photomicrographs. **(a)** Plane-polarized image of a thin section of sample MM30 with the location of the plane- and cross-polarized images shown in **(b)**, **(c)**, and **(d)** indicated. **(b)** K-feldspar and quartz grains showing irregular grain boundaries. **(c)** Biotite grains with scalloped edges and finer-grained intergrowths of K-feldspar and plagioclase. **(d)** The edge of a garnet grain with thin films of K-feldspar.

and milled using a steel swing mill. Major element analysis was conducted on fused beads using a Malvern-Panalytical Zetium 3.0 kW RH-tube WD-XRF.

3.4 Mineral chemistry

Another large garnet from the sample MM31 was prepared as a thin section, and several regions with smaller garnets were also prepared as thin sections. The garnet epoxy mounts were imaged (Fig. 5) using a Bruker Micro-XRF M4 Tornado hosted at the Geological Survey of Finland (GTK). The system is equipped with a 30-Watt rhodium (Rh) anode X-ray tube, two $30\,mm^2$ silicon drift detectors (SDDs) with an energy resolution of $< 145\,eV$ (MnKα) at 275 kcps (kilocounts per second) via beryllium windows and poly-capillary optics. All data acquisition was performed with an accelerating voltage of 50 kV, a beam current of 500 µA using a fixed spot size of 20 µm under a 2 mbar vacuum. The samples were measured in a single run using a step size of 40 µm and a pixel dwell time of $20\,ms\,px^{-1}$. The qualitative elemental maps were generated using the Bruker M4 software with later processing in XMapTools (Lanari et al., 2014). Quantified chemical analysis (Table S2 and S3 in the Supplement) of major minerals (garnet, biotite, K-feldspar, and plagioclase) using the thin-section samples were obtained using a CAMECA SX100 electron microprobe analyser (EMPA) at GTK using the WDS (wavelength-dispersive) technique. The accelerating voltage and beam current were set to 15 kV and 15 nA, respectively. A defocused beam diameter of 5 µm was used for the spot analysis. Analytical results have been corrected using the PAP online correction program (Pouchou and Pichoir, 1986). Natural minerals and synthetic metals were used as standards. All mineral chemical data are included in the Table S2 and S3.

3.5 Garnet and apatite in situ Lu–Hf geochronology

Two garnet-bearing samples (large garnet within leucosome with apatite inclusions, MM31, and small mesosome garnet, MM30) were analysed using polished epoxy mounts (Fig. 5) for in situ Lu–Hf garnet and apatite geochronology at Adelaide Microscopy, University of Adelaide, Australia. Garnet and apatite Lu–Hf dating was conducted over two analytical sessions using a RESOlution-LR 193 nm excimer laser ablation system, coupled to an Agilent 8900 ICP-MS/MS. The laser beam diameter was set to 173 µm (garnet) and 120 µm (apatite), and ablation was conducted at 10 Hz repetition rate and a fluence of $\sim 3.5\,J\,cm^{-2}$.

The laser-based Lu–Hf method uses a NH_3–He gas mixture in the reaction cell of the mass spectrometer to promote high-order reaction products of Hf, with a mass shift of $+82$, while equivalent Lu and Yb reaction products are minimal (i.e. Hf reacts at a rate of 50 %–60 %, while Lu reacts at < 0.003 %; Simpson et al., 2021). Consequently, the resulting mass-shifted ($+82$ amu) reaction products of $^{176+82}$Hf and $^{178+82}$Hf can be measured free from isobaric interferences. In addition, ^{177}Hf was subsequently calculated from ^{178}Hf, assuming natural abundances, while ^{175}Lu was measured on mass as a proxy for ^{176}Lu (see details in Simpson et al., 2021, 2023). In addition to Lu and Hf isotopes, other trace elements, including a selection of other Rare Earth elements (REEs) (details in Table S5), were measured simultaneously to monitor for inclusions and to characterize the nature of the fluids. However, not every REE was measured, as this would compromise the dwell times on the Hf isotopes required for age calculations. For both garnet and apatite Lu–Hf analysis, NIST 610 was used as a primary reference material (Nebel et al., 2009). For garnet, the reference material Högsbo garnet (reference age 1029 ± 1.7 Ma) was analysed repeatedly to correct for matrix-dependent fractionation (Simpson et al., 2021; Glorie et al., 2024b), and secondary garnet reference material BP-1 (Black Point, South Australia; Glorie et al., 2024b) was used to validate the accuracy of the Lu–Hf dates. BP-1 produced a garnet Lu–Hf isochron age of 1749 ± 15 Ma (Table S4), which is consistent with the published monazite U–Pb age of 1745 ± 14 Ma (Lane, 2011).

For apatite, the reference material OD-306 was analysed repeatedly to correct for matrix-dependent fractionation (1597 ± 7 Ma; Thompson et al., 2016). The secondary reference apatites Bamble-1 (Bamble sector, SE Norway, Lu–Hf age of 1102 ± 5 Ma; Glorie et al., 2024a) and HR-1 (Harts Range, N Australia, Lu–Hf age of 343 ± 2 Ma; Glorie et al., 2022) were used to monitor accuracy. During this study the age obtained was 1084 ± 18 Ma for Bamble-1 and 344 ± 3 Ma for HR-1 (Table S5). Apatite U–Pb and trace element analysis was conducted on the same instrumentation as for the Lu–Hf analyses, using identical analytical parameters to those in Gillespie et al. (2018) and Glorie et al. (2019), including a laser diameter of 30 µm and repetition rate of 5 Hz. The primary reference material used was MAD (ID-TIMS, U–Pb age 473.5 ± 0.7 Ma; Thomson et al., 2012; Chew et al., 2014). The 401 apatite was used as a secondary standard, producing a weighted mean ^{206}Pb/^{238}U age of 529 ± 2 Ma (Table S6). This is in good agreement with the published age (ID-MC-ICP-MS, U–Pb age 530.3 ± 1.5 Ma; Thompson et al., 2016).

Isotope ratios and trace element concentrations were calculated in LADR (Norris and Danyushevsky, 2018). Lu–Hf ages were calculated as inverse isochrons using IsoplotR (Vermeesch, 2018; Li and Vermeesch, 2021) with the ^{176}Lu decay constant of Söderlund et al. (2004) 0.0001867 ± 0.00000008 Ma^{-1}. For samples that produced exclusively high radiogenic ^{177}Hf/^{176}Hf ratios ($< \sim 0.1$), the isochron was anchored to an initial ^{177}Hf/^{176}Hf composition of 3.55 ± 0.05, and this value spans the entire range of initial ^{177}Hf/^{176}Hf ratios of the terrestrial reservoir (e.g. Spencer et al., 2020). All presented ages have absolute errors at the 2 SD level.
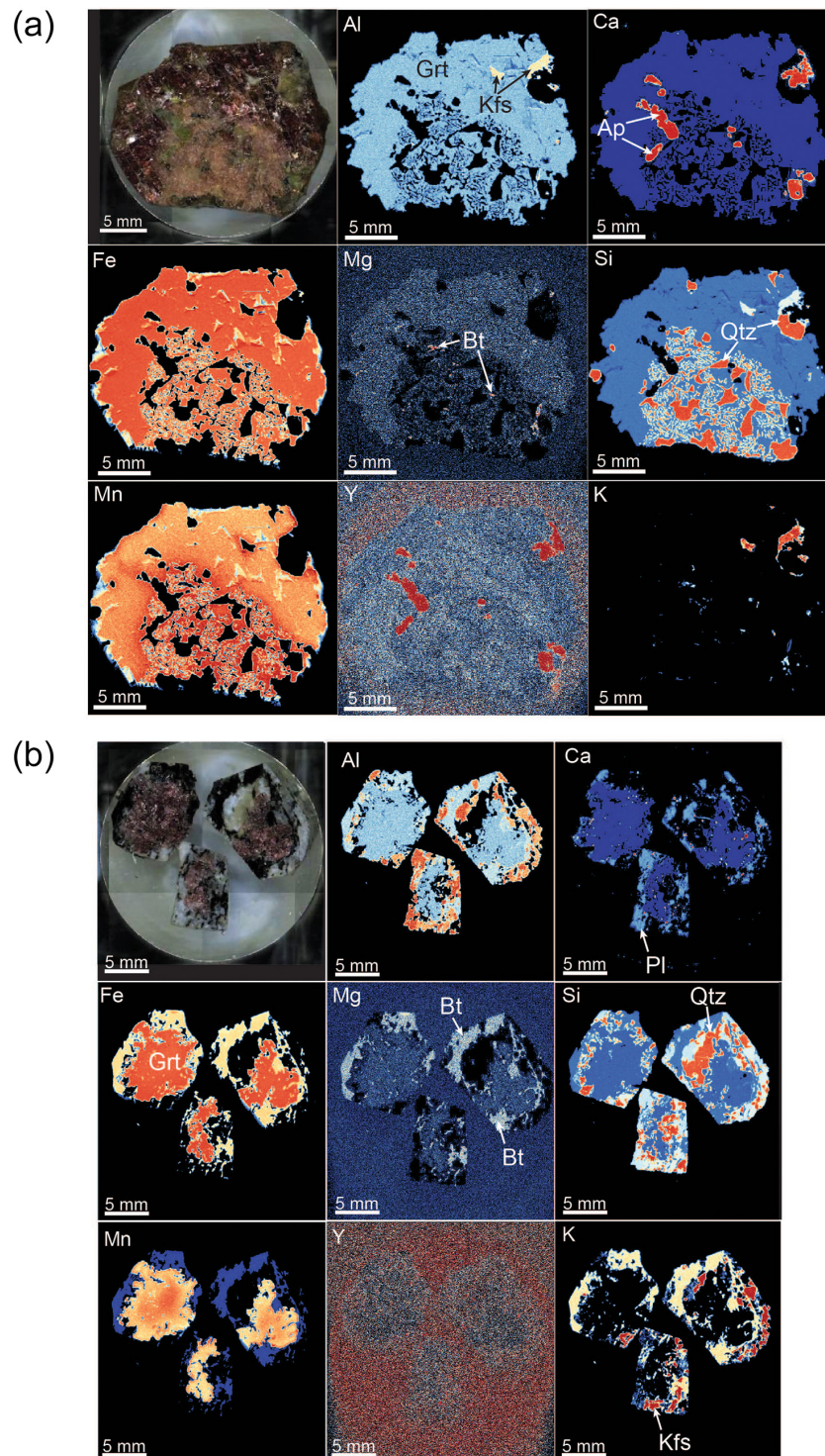
Figure 5. (a) Garnet from leucosome (MM31) mounted in epoxy with elemental images of the mount obtained by micro-XRF. Images are intensity maps, with the colour scale varying from black and blue (low) to red (high). **(b)** Garnet grains from the mesosome (MM30) mounted in epoxy with elemental images of the mount obtained by micro-XRF. Images are intensity maps, with the colour scale varying from black and blue (low) to red (high).

3.6 Pressure–temperature pseudo-section modelling

Pressure–temperature pseudo-sections were calculated for sample MM30A using the software package Theriak/Domino (de Capitani and Petrakakis, 2010) and the database of Holland and Powell (2011) for the geologically realistic system MnNCKFMASH (MnO–Na$_2$O–CaO–K$_2$O–FeO–MgO–Al$_2$O$_3$–SiO$_2$–H$_2$O). The "metapelite set" of models from White et al. (2014a), converted to Theriak/Domino format by Doug Tinkham (see Jørgensen et al., 2019) were applied. These are White et al. (2014b) for orthopyroxene, garnet, biotite, staurolite, chloritoid, cordierite and chlorite; White et al. (2014a) for muscovite and silicate melt; Holland and Powell (2011) for epidote; and Holland and Powell (2003) for plagioclase. Quartz, H$_2$O, kyanite, sillimanite, and andalusite are also included as pure phases. Due to the large amount of Mn present in the garnet, MnO was included in the system. However, the low Ti content and absence of Ti-bearing minerals makes the inclusion of TiO$_2$ unnecessary. Additionally, a lack of Fe^{3+}-bearing phases such as magnetite and the low indicated Fe^{3+} contents in recalculated garnet analysis (see Table S2) indicated that including ferric iron in the modelling was unnecessary.

The presence of leucosomes, fine-grained domains, and cuspate grain boundaries in sample MM30A suggest that melt was part of the peak assemblage of the samples. Since it is impossible to know if this melt was retained in the system, a $T - X_{H_2O}$ diagram was calculated to indicate an appropriate H$_2$O value for the P–T diagram (Fig. S1). Many thin sections contain a significant amount of apatite, which is also observed as inclusions within garnet (Fig. 5a). Since apatite contains appreciable amounts of CaO, a $T - X_{CaO}$ diagram was also generated using the measured amount of P$_2$O$_5$ to determine the maximum amount of CaO that could be attributed to apatite (Fig. S2).

4 Results

4.1 Whole-rock geochemistry

To further support this research, 117 whole-rock intermediate and felsic geochemical analyses of the Olkiluoto site TGG were compiled from Kärki and Paulamäki (2006), including metatexites and diatextites and injected pegmatitic granites and leucosome veins (Table S7). The diabase dykes from the Olkiluoto region were excluded from the dataset because the dykes intruded into the bedrock considerably later than the period when the main part of the bedrock was formed. Figure 6 shows the main whole-rock compositional characteristics of the Olkiluoto site rocks, distinguishing between typical TGGs and high-P TGGs. Geochemical discrimination diagrams such as TAS (Fig. 6a) show the difference between normal dominant TGGs (SiO$_2$ 49.60 wt %–77.83 wt % and P$_2$O$_5$ 0.10 wt %–0.23 wt %) and high-P

TGGs (SiO$_2$ 48.45 wt %–67.57 wt % and P$_2$O$_5$ 0.31 wt %–1.73 wt %) (Fig. 6). In addition, AFM diagrams effectively illustrate this distinction with high-P TGGs following the tholeiitic series trend, indicative of an older protolith part of migmatites with mainly lower SiO$_2$ contents, and most of the TGGs following a calc-alkaline series trend typical of arc environments fitting well to Svecofennian orogeny (Fig. 6b).

4.2 Major-element and trace element mineral chemistry

Garnet major-element mineral chemistry is very similar in terms of trends and absolute values for the large (MM31) and small (MM30) grains (Fig. 7). Garnet from both MM31 and MM30 has significant iron enrichment, with X_{Alm} ($= Fe/(Fe + Mn + Mg + Ca)$) of 0.77 to 0.80. In the large garnet grains, X_{Alm} is fairly constant across the grain, with slight increases next to quartz inclusions. In the small garnet grains, X_{Alm} is slightly elevated both in the core (0.79) and the rim (up to 0.80; Fig. 7b). X_{Pyr} ($= Mg/(Fe + Mn + Mg + Ca)$) values range between 0.08 to 0.12, with the lowest values found in grain cores (0.08) and directly adjacent quartz inclusions. The highest X_{Pyr} values (0.12) are from the rim, although the X_{Pyr} content drops abruptly right at the edge of the grain (Fig. 7b, d). The same patterns are observed in both large and small garnet grains (Fig. 7). X_{Sps} ($= Mn/(Fe + Mn + Mg + Ca)$) values vary from 0.11 to 0.08, with the higher values coming from the grain core, directly adjacent to quartz inclusions, and at the grain rim (Fig. 7). A similar pattern is observed in both large and small garnet grains (Fig. 7). X_{Grs} ($= Ca/(Fe + Mn + Mg + Ca)$) values exhibit flat profiles in both large and small garnet grains, with a constant value of just over 0.02. The micro-XRF maps indicate similar compositional variations, with mostly uniform Fe, Mg, and Ca (Fig. 5). The Mn maps show higher values in the core, around quartz inclusions, and at the rim of grains. The Y map of the large garnet clearly shows the location of high-Y apatite inclusions, which are mostly hosted at the rims of large garnet grains (Fig. 5a). The larger garnet seems to have higher Y contents than the small garnet grains. The rim zone, being inclusion poor, appears to have higher Y than the quartz-dominated garnet core; however, Y contents collected during Lu–Hf analysis indicate higher values for the grain core (Fig. 5a; Table S4). The small garnets appear to be uniformly low in Y content (Fig. 5b).

Biotite grains, aligned parallel to the compositional layering, have X_{Mg} ($= Mg/(Mg + Fe)$) values of 0.34 to 0.37, with higher values observed in grains included in garnet. TiO$_2$ content varies from 1.84 wt % to 2.88 wt %. In the large garnet sample, plagioclase exhibits a variable composition with X_{Ab} ($= Na/(Na + Ca + K)$) of 0.76 to 0.96. The sample with small garnet has a more restricted X_{Ab} of 0.74–0.79. K-feldspar is dominantly K-rich with X_K ($= K/(Ca + Na + K)$) of 0.81 to 0.87 in both the small and large garnet samples.
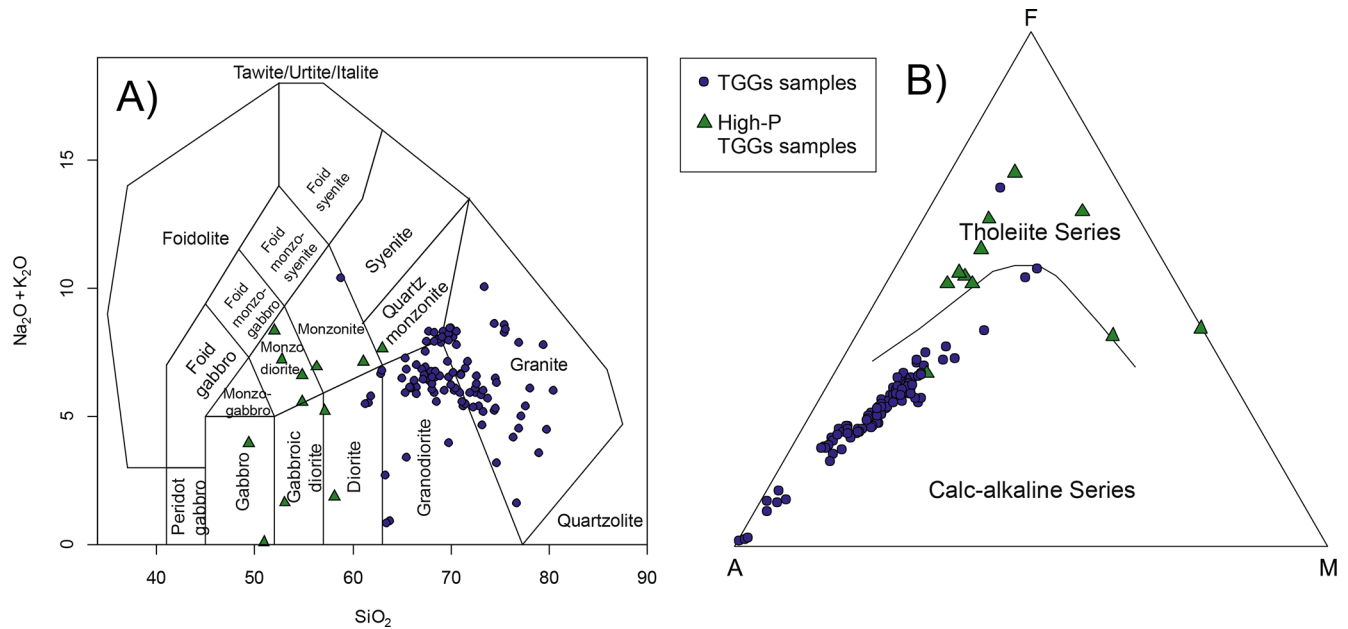
Figure 6. The whole-rock geochemistry from Olkiluoto region. **(a)** TAS diagram after Middlemost (1994). **(b)** AFM diagram after Irvine and Baragar (1971). Lithologies are divided in two types as follows: the dominant TGG (tonalitic–granitic–granodioritic) rock with migmatites including metatexites and diatexites and high-*P* TGG (tonalitic–granitic–granodioritic) rock..

4.3   Garnet in situ Lu–Hf geochronology

Two garnet samples (MM30 and MM31) were targeted for in situ Lu–Hf geochronology: one large garnet (MM31) hosted in a leucosome and three small grains (MM30) obtained from the mesosome. From the large grain (MM31), a total of 84 analyses were conducted, with 42 targeting the grain core and 42 at the grain rim (see Fig. S3 for spot locations). Two analyses were excluded from the age calculations due to the presence of inclusions. When all the data are plotted on an isochron anchored to an initial $^{177}Hf/^{176}Hf$ ratio of 3.55 ± 0.06 (covering the range of terrestrial values; Mark et al., 2023), the result is an isochron age of 1829 ± 19 Ma ($n = 83$, MSWD $= 1.2$; Fig. 8a; one analysis was duplicated with different segments of the signal selected; Table S4). Analyses obtained from the grain core have a larger spread in $^{176}Lu/^{176}Hf$ ratios, yielding an age of 1828 ± 11 Ma ($n = 43$, MSWD $= 1.3$; one analysis was duplicated with different segments of the signal selected; Fig. S4), whereas the measurements from the garnet rim data give an identical isochron age with a larger uncertainty of 1828 ± 21 Ma ($n = 40$, MSWD $= 1.1$; two data points were excluded due to inclusions; Fig. S5). Garnet cores have Lu contents of 10 to 7 ppm (average is 35 ppm) when calibrated to an internal standard of 12 wt % Al. Garnet rims have Lu contents of 10 to 25 ppm (average is 18 ppm).

The small garnet grains were targeted with 51 analyses in total (see Fig. S6 for spot locations) and have a restricted $^{176}Lu/^{176}Hf$ ratio range, resulting in an anchored isochron age of 1857 ± 49 Ma ($n = 51$, MSWD $= 1.1$; Fig. 8b). If the

grains are plotted separately, they all produce the same age within uncertainty, but the errors are larger due to the smaller number of analyses. The small garnets have Lu contents ranging from 10 ppm to below the detection limit (average is 4 ppm).

4.4   Apatite Lu–Hf and U–Pb geochronology

Four apatite inclusions in the rim of the large garnet (MM31) were dated using both Lu–Hf and U–Pb methods in two separate analytical sessions. The Lu–Hf data are mostly highly radiogenic (38 of 47 analyses with $^{177}Hf/^{176}Hf$ ratios < 0.1) and define an anchored Lu–Hf isochron age of 1782 ± 19 Ma (MSWD $= 1.6$; Fig. 9a). Alternatively, calculating a weighted-mean common-Hf-corrected Lu–Hf age (for apatites with $^{177}Hf/^{176}Hf$ ratios < 0.1) returns a similar age within uncertainty of 1784 ± 8 Ma (MSWD $= 1.3$, $n = 38$). The apatite REE spidergrams indicate slightly enriched light REEs, a pronounced negative Eu anomaly, and flat HREE profiles (Fig. 9c). The investigated apatite compositions plot in the HM field of the apatite classification biplot of O'Sullivan et al. (2020), indicating apatite crystallized during partial high-grade metamorphic melting processes (Fig. 9d). The apatite U–Pb data plot on a linear trend with some slight scatter (Fig. 9b). An isochron based on 40 out of 45 analyses produces a lower intercept age of 1778 ± 16 Ma (MSWD $= 0.41$). The five analyses excluded from this isochron could be related to partial inheritance from an older event or isotopic disturbance (U loss; Fig. 9b).
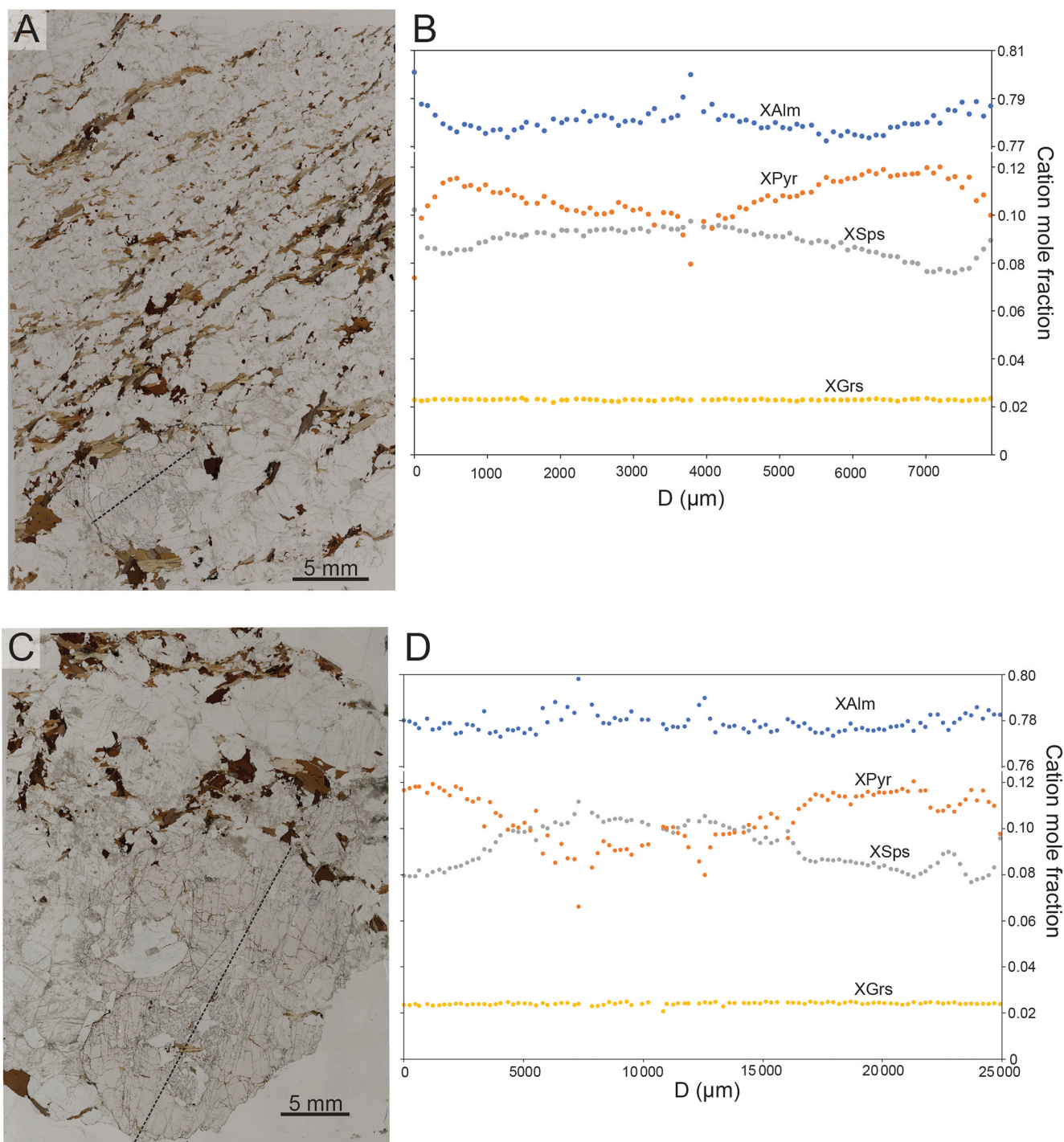
Figure 7. Garnet major-element zonation. **(a)** Plane-polarized image of a thin section of the mesosome domain including the location of a small garnet grain (MM30) used for the EPMA traverse. The location of the traverse is indicated with the thin dashed line. **(b)** Garnet traverse for the grain in Fig. 7a. The traverse starts from the left side of the garnet grain. **(c)** Plane-polarized image of a thin section from the leucosome with a large garnet grain (MM31). The location of the traverse is indicated with the thin dashed line. **(d)** Garnet traverse for the grain in Fig. 7c. The traverse starts from the left side of the garnet grain.
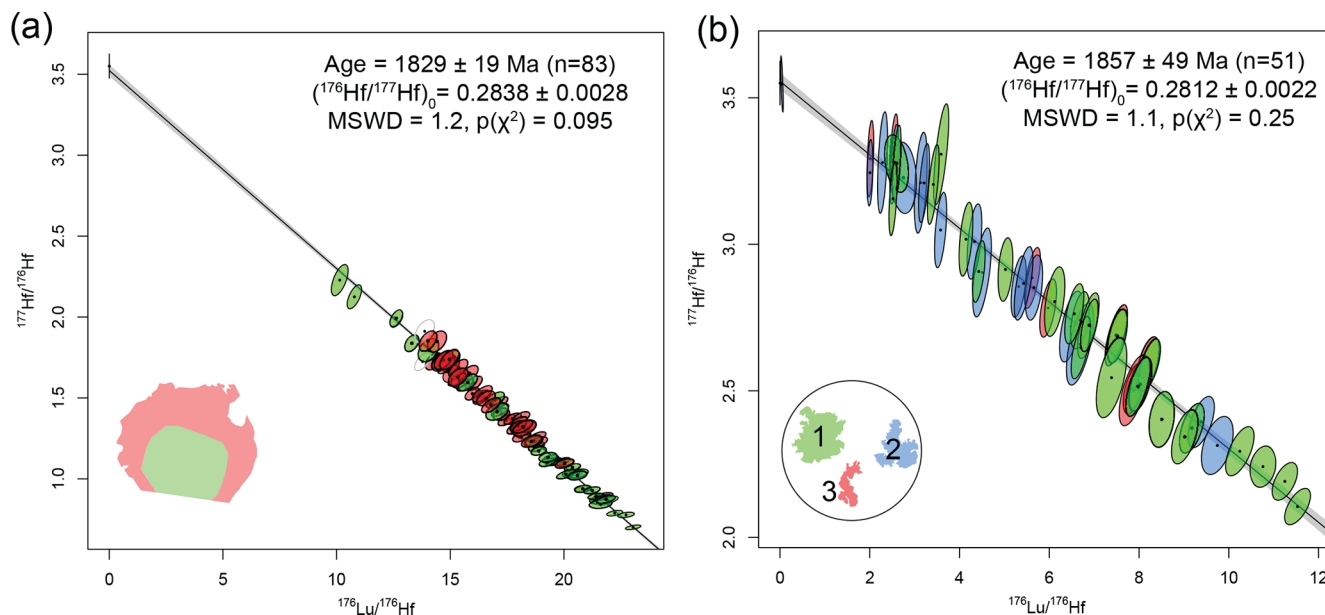
Figure 8. (a) Lu–Hf inverse isochron for the large garnet sample (MM31). Analyses are coloured based on their location within the garnet grain (green for the core, and red for the rim). **(b)** Lu–Hf inverse isochron for the small-garnet sample (MM30). Analyses are coloured based on which garnet grain they were obtained from (see the inset for the colour key).

4.5 Pressure–temperature pseudo-section modelling

For sample MM30A, the $T - X_{H_2O}$ diagram (Fig. S5) indicates that the interpreted peak assemblage of garnet + plagioclase + K-feldspar + biotite + quartz + melt is present at H_2O contents > 0.25 on the binary diagram. For this reason, H_2O was set at 0.3 for further calculations corresponding to a H_2O content of less than 1 wt %. A $T - X_{CaO}$ diagram was calculated to investigate the impact of apatite on the whole-rock CaO content. The diagram was created using the whole-rock composition on one side, with the other side indicating a reduction in CaO using the P_2O_5 content of the whole rock to indicate the maximum amount of CaO attributable to apatite. In the $T - X_{CaO}$ diagram, the interpreted peak assemblage occurs only on the right side of the diagram, suggesting that only a modest amount of CaO (corresponding to a 25 % reduction) needs to be removed to account for apatite in the sample. Thus, the $P–T$ diagram for sample MM30A was calculated at 0.75 of the $T - X_{CaO}$ diagram (indicating that of a total 100 % CaO that could be attributed to apatite, only 25 % was removed; see Fig. S2).

The $P–T$ diagram for sample MM30A has the interpreted peak assemblage field of garnet + plagioclase + K-feldspar + biotite + quartz + melt present over a large range of pressures and temperatures, extending from 2.5 kbar to over 10 kbar and from 650 to 800 °C (Fig. 10). The garnet compositional isopleths that correspond to the garnet compositional range observed in both the large and small garnet grains (X_{Alm}: 0.8–0.78; X_{Pyr}: 0.12–0.1; X_{Sps}: 0.1–0.08; $X_{Grs} < 0.04$; Fig. 7) occur in the low-pressure part of the

field with compositional overlap occurring in the range of 3–5 kbar and ca. 700 °C (Fig. 10).

5 Discussion

5.1 Significance of the age data and metamorphic constraints

The small-garnet (MM30) Lu–Hf data produce an age of 1857 ± 49 Ma with a large uncertainty as a result of the low Lu contents in the small garnet. The analyses from the large garnet (MM31) produce a Lu–Hf age of 1829 ± 19 Ma. These results are statistically indistinguishable, meaning that if there is a difference in age between the small and large garnets, it is not possible to define this with the Lu–Hf method. To distinguish these populations, more data are required targeting high-Lu domains within the small mesosome garnets or obtaining additional samples. Texturally, the small garnets occur in the rock mesosome, while the larger garnets occur in the leucosome. This may mean that the smaller garnets are older. However, both the sample mesosomes and leucosomes are deformed by the same foliation (Figs. 3, 4, 7), suggesting it is equally feasible that all garnet grew in response to a single phase of deformation. The mesosome garnets may be small due to having a limited equilibrium volume in comparison with the leucosome garnet that formed in melt. This may also be responsible for the variable Lu contents. The small mesosome garnets have the lowest Lu contents (average of 4 ppm), potentially due to a small equilibrium volume. The leucosome garnets growing in melt may
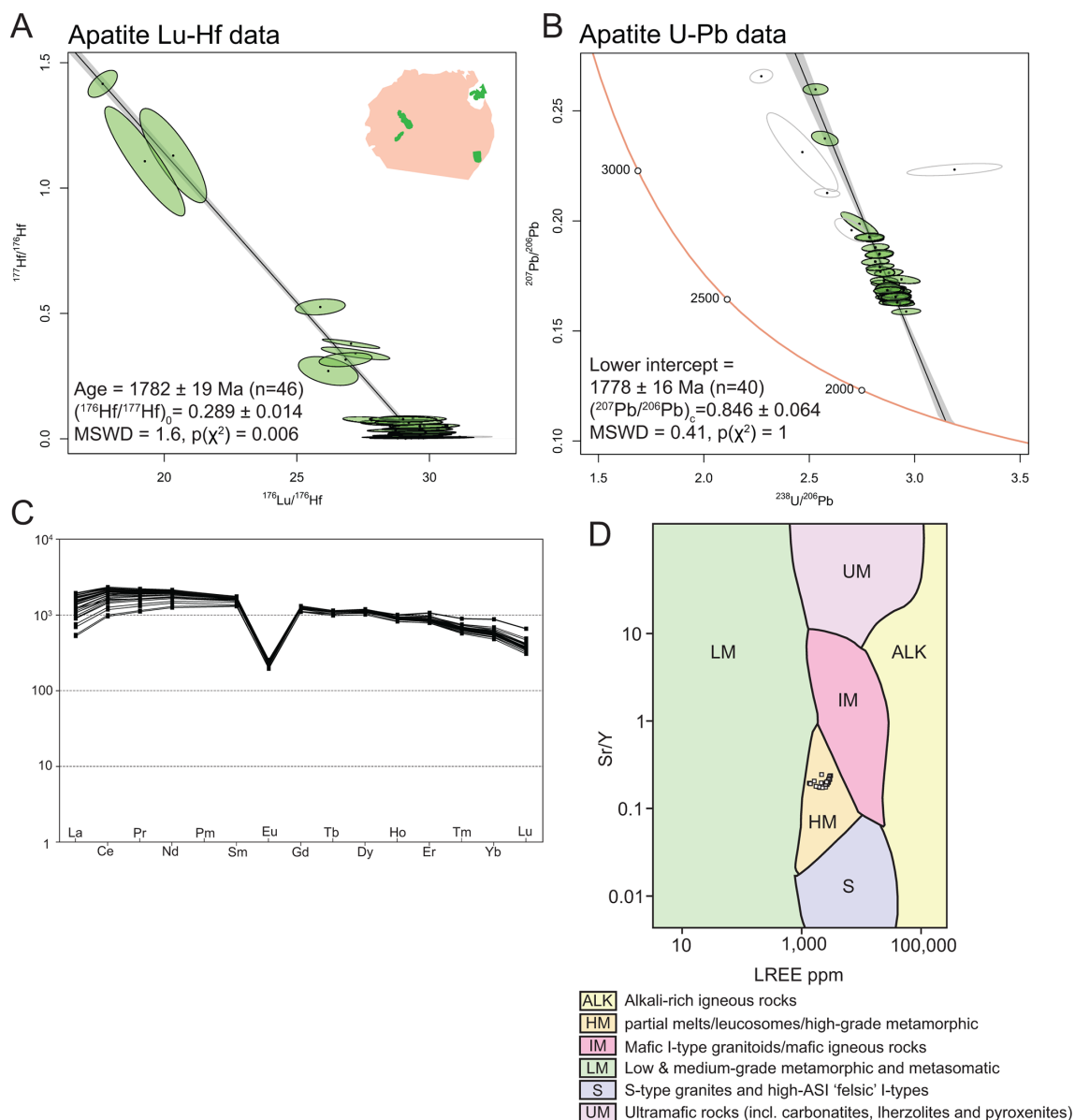
Figure 9. (a) Lu–Hf inverse isochron for apatite occurring within the large garnet grain (green grains in the inset image). **(b)** Apatite U–Pb data plotted on a Terra–Wasserburg concordia plot. **(c)** Apatite REE spidergram normalized to chondrite (McDonough and Sun, 1995). **(d)** Apatite classification biplot of O'Sullivan et al. (2020) based on Sr–Y vs. $\sum$LREE (La–Nd). The apatite analysed in this study is plotted on this diagram as small white squares and plots exclusively in the HM field.

have had a larger equilibrium volume due to more effective transport of elements within the melt, resulting in the highest Lu contents in the grain cores (average of 38 ppm) with lower values in the rim (average of 21 ppm) following garnet (and melt) crystallization. An additional support for this scenario is the largely flat major-element zonation of both large and small garnets with similar absolute values. This would indicate that both small and large garnets equilibrated at the same elevated T conditions. Thus, based on our current results we interpret that the large garnets and possibly also the small garnets grew in response to one metamorphic

event at 1829 ± 19 Ma (MSWD of 1.3) using the age obtained from the large leucosome garnet (MM31). Recently, Smit et al. (2024) showed that even at high-grade conditions ($> 800\,°C$), REE diffuse slowly in natural garnet, making Lu–Hf chronology extremely robust. Despite a long and complex history of upper amphibolite facies metamorphism and magmatism in the region (Väisänen and Hölttä, 1999; Hölttä and Heilimo, 2017; Torvela and Kurhila, 2020), it is likely that the Lu–Hf results reflect garnet growth ages.

The Lu–Hf and U–Pb ages obtained for apatite grains hosted inside large garnets are similar within error, producing
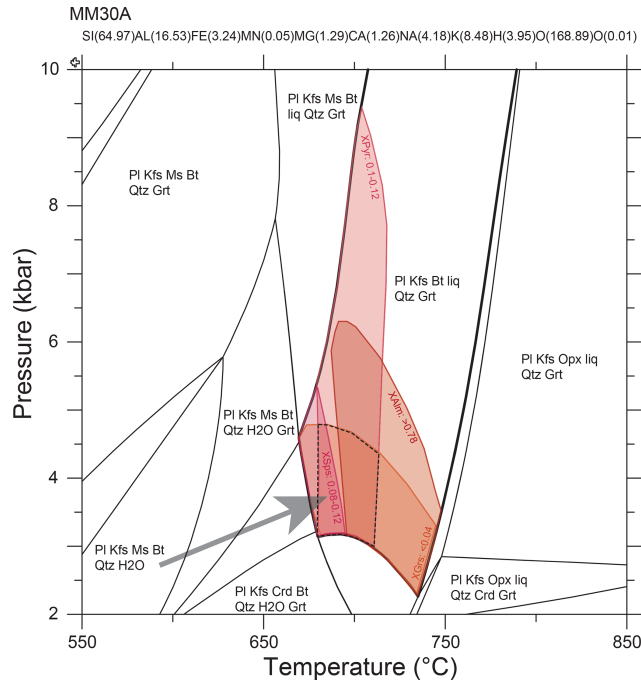
Figure 10. P–T pseudo-section for sample MM30A using the bulk composition shown at the top of the diagram (see Table S1). The $T - X_{H_2O}$ and $T - X_{CaO}$ diagrams used to investigate this composition are given as Figs. S5 and S6. The shaded red areas indicate regions matching the garnet composition observed in the sample (X_{Alm}: 0.8–0.78; X_{Pyr}: 0.12–0.1; X_{Sps}: 0.1–0.08; $X_{Grs} < 0.04$). The dashed black box is the field of overlap in the P–T pseudo-section, and the grey arrow indicates the direction of increasing garnet mode (see Fig. S7).

ages of 1782 ± 19 and 1778 ± 16 Ma, respectively. The Lu–Hf system in apatite is considered to have a higher closure temperatures (~ 670–$730\,°C$; Glorie et al., 2024a) than U–Pb in apatite (350–$570\,°C$; Chew and Spikings, 2021). Thus, a similarity in the U–Pb and Lu–Hf ages is indicative of fast cooling at the time of apatite growth. The difference in age between the apatite and the hosting garnet grain (large garnet gave an isochron age of 1829 ± 19 Ma) could indicate that the apatite grains are in contact with the mesosome and the symplectitic quartz that occurs in the grain core (thus open to grain boundary fluid conduits that may have resulted in resetting at ca. 1780 Ma) or alternatively that the sample may have stayed at an elevated temperature ($> 700\,°C$) from ca. 1830 to 1780 Ma. This would be consistent with the relatively flat major-element compositional profiles in garnet. Producing nearly flat profiles in a large garnet grain would require a prolonged period (likely on the order of tens of millions of years) at temperatures above $650\,°C$ (Caddick et al., 2010).

Mänttäri et al. (2006) obtained U–Pb zircon and monazite ages from the same TGG gneiss unit sampled in this study (sample site 2006 in Fig. 2). The zircon U–Pb data indicate a crystallization age of ca. 1860 Ma for the tonalite with

Archean (ca. 2.7 Ga) and Paleoproterozoic (2.0–1.9 Ga) inheritance. Pegmatitic granite dykes, interpreted to be related to a migmatization (partial melting) event, yield zircon ages of ca. 1830–1790 Ma with interpreted inheritance of Archean (ca. 2.7 Ga) and ca. 1865 Ma. A monazite U–Pb age from a pegmatite of 1823 ± 3 Ma is interpreted as a minimum age for pegmatitic dykes (Mänttäri et al., 2006), and these are ages consistent with the dates obtained in this study and are interpreted as ages for the high-temperature partial melting event.

The P–T diagram for sample MM30A indicates peak P–T conditions at 3–5 kbar and $\sim 700\,°C$. This result is consistent with previous studies at the Olkiluoto site by Tuisku and Kärki (2010), defining that migmatization of pelitic gneisses due to the dehydration melting of biotite, sillimanite, plagioclase, and quartz in the temperature between 660 to $700\,°C$ and pressure of 3.5–4 kbar. The arrow in Fig. 10 indicates a proposed prograde P–T path defined by the increase in garnet mode. The P–T path is also parallel to grossular compositional isopleths, producing flat compositional zonation in X_{Grs} along this path, as well as an increase in X_{Pyr} and decrease in X_{Sps} consistent with the compositional zonation observed in the sample.

Based on the interpretation above, the garnet ages likely represent growth ages, representing a period of prograde evolution that occurred at 1829 ± 19 Ma. The large apatite grains that occur as inclusions at the rim of the large garnet preserve Lu–Hf and U–Pb ages of 1782 ± 19 and 1778 ± 16 Ma. As discussed above, this presents two options for the metamorphic evolution of the sample. Either the sample cooled from peak conditions at ca. 1830 Ma, which then reheated to nearly identical conditions at ca. 1780 Ma, or high-temperature conditions persisted from 1830 to 1780 Ma, at which point rapid cooling from 700 to 400–500 °C (closure T of U–Pb in apatite) occurred. The latter metamorphic evolution would be consistent with a regional high-temperature–low-pressure event that in other areas has been interpreted to have persisted for this period (Hölttä and Heilimo, 2017). These conditions potentially persisted for ca. 50 to ca. 1780 Ma, where the transition from ductile to brittle tectonics has been inferred by Torvela et al. (2008). The study by Nordbäck et al. (2022) from the Olkiluoto site concluded that the ductile to brittle transition was related to the late Svecofennian tectonics, where structurally controlled accumulation and percolation of metamorphic fluids occurred in ductile shear zones that in turn finally triggered the first embrittlement in Olkiluoto and emplacement of quartz veins in faults.

5.2 The role of Olkiluoto region in the tectonic setting of southern Finland

The P–T–t conditions of Olkiluoto are summarized in Fig. 11, and a comparison to surrounding Svecofennian tectonic belts is shown. The Tampere Belt experienced greenschist (central Tampere Belt) to amphibolite (east and west Tampere Belt) facies conditions with peak metamorphism interpreted to occur at ca. 1.88 Ga (Mouri et al., 1999). Lahtinen et al. (2017) also obtained a garnet age from a mica schist in the Tampere Belt producing an age of 1.81 Ga, which they suggest indicates that elevated temperature conditions continued until this time. The Pirkanmaa Belt contains upper amphibolite to granulite facies migmatitic rocks that experienced peak metamorphic conditions at 4–5 kbar and 750–700 °C at ca. 1.88 Ga (Mouri et al., 1999). There is also evidence of younger monazite (ca. 1.85 Ga, Hölttä et al., 2020) and a range of garnet Sm–Nd ages from 1.89–1.84 Ga (Lahtinen et al., 2017; Mouri et al., 1999). The Häme Belt metapelitic rocks are either sillimanite–muscovite gneisses or schists, whose Al-rich layers often have andalusite, staurolite, or even cordierite porphyroblasts. The estimated P–T conditions on the basis of these stable mineral assemblages is inferred during the peak metamorphism to be 3–4 kbar and 530–580 °C (Hölttä and Heilimo, 2017). The age of peak metamorphism is poorly defined but is generally interpreted to have occurred at 1.83–1.80 Ga based on U–Pb zircon and titanite ages in altered diorite (Saalmann et al., 2010; Hölttä et al., 2020). Saalmann et al. (2009) indicate that the Häme Belt experienced an earlier compressional event at ca. 1.88–1.86 Ga by subduction, followed by an extensional event caused by a slab rollback event. This is supported by the study from Lahtinen et al., (2017) that found 1.90–1.86 Ga metamorphic overgrowth in zircons from a metapsammitic rock. The southernmost Uusimaa Belt is proposed to have experienced crustal extension at 1.86–1.84 Ga, followed by a transpressional event producing granulite facies peak conditions of 4–7 kbar and 750–825 °C at 1.83–1.80 Ga (Väisänen and Hölttä, 1999; Mouri et al., 2005; Skyttä and Mänttäri, 2008).

The Olkiluoto region and the Häme Belt (situated ca. 75 km southeast from Olkiluoto; Fig. 11) have similar crystallization ages (Kähkönen, 2005; Mänttäri et al., 2006) and metamorphic and tectonic histories during the ca. 1.88–1.79 Ga Svecofennian orogeny. Previous metamorphic studies in the Häme Belt have shown that it contains supracrustal rocks that have been interpreted to have two metamorphic peaks: the first in amphibolite facies conditions at ca. 1.88–1.86 Ga (Nironen, 1999; Väisänen et al., 2002; Kähkönen, 2005; Kara et al., 2021) and the latter during a high-T event that peaked at ca. 1.83–1.81 Ga (Väisänen et al., 2002). Kurhila et al. (2011) determined that southern Finland was subjected to a prolonged anatexis event and a later event with the emplacement of late-orogenic leucogranites, while Torvela and Kurhila (2022) determined that, in addition to a

hot anatexis, a late-orogenic event was coupled to migmatization and formation of major shear zones in a transpressional tectonic regime (Fig. 11). Our novel garnet and apatite Lu–Hf age data, together with apatite U–Pb age data, that are coupled with pseudo-section modelling and supporting data from the previous study on the structural setting by Engström et al. (2022), support the same evolution for the Olkiluoto region and the Häme Belt. Thus, the ages indicated by the Lu–Hf geochronology (1829 ± 19 Ma) of the garnet samples from this study are interpreted to show the later distinct metamorphic peak (M2) for the Olkiluoto site. The later metamorphic peak (M2) caused migmatization of the Olkiluoto site's protolith tholeiitic TGG rocks, which have a high P2O5 content, resulting in the formation of dominant calc-alkaline series TGG rocks via anatexis during this period (see Sect. 4.1). Additionally, the structural study by Engström et al. (2022), that states that the pegmatitic leucosomes (M2) that formed later crosscut earlier compositional banding, implying that they are younger, while the metamorphic evolution in this study infers similar metamorphic and tectonic signatures to other studies from the Häme Belt (Kähkönen, 2005; Hölttä and Heilimo, 2017; Kara et al., 2021; Lahtinen et al., 2023).

The study by Saalmann et al. (2009) determined that the observed metamorphic peak in the Häme Belt was followed by a hydrothermal event with formation of shear zones and mineralization. Even though no mineralization indicative of a hydrothermal event is observed in the Olkiluoto site, a similar hydrothermal and shearing-induced event is exemplified by the formation of a certain type of diatexitic migmatite with roundish quartz feldspar megacrysts (Engström et al., 2022), which are interpreted to be related to the prolonged cooling after the peak P–T conditions of 3–5 kbar and around 700 °C (this study). The ductile–brittle transition at the Olkiluoto site is interpreted to be related to metamorphic fluids and the roundish quartz feldspar megacrysts are determined to have a tectonic connection to the first brittle tectonic faulting event in Olkiluoto (Engström et al., 2022; Nordbäck et al., 2022). Thus, it is plausible that latest tectonic hydrothermal and shearing-induced events in the Häme Belt and at the Olkiluoto site could be syn-tectonic.

At the same time, the Uusimaa Belt (Fig. 11) mainly underwent granulite facies metamorphism at ca. 1.84–1.81 Ga (Väisänen et al., 2002; Mouri et al., 2005; Skyttä and Mänttäri, 2008), inferring slightly deeper crustal depth than the Häme Belt. These belts and the Olkiluoto site seem to have a similar geothermal gradient, where the Uusimaa Belt, Häme Belt, and Olkiluoto site have geothermal gradients of 63, 57, and 64 °C km^{-1}, respectively (based on P–T estimates and crustal density of 2.75 g cm^{-3}). The interpretation further south in the Uusimaa Belt, where shear zones and the anatectic melting are strongly coupled to each other (Torvela and Kurhila, 2020; Lahtinen et al., 2023), indicates that the whole of the southern Finland domain was subjected to a long hot orogenic evolution with several crustal-scale melt
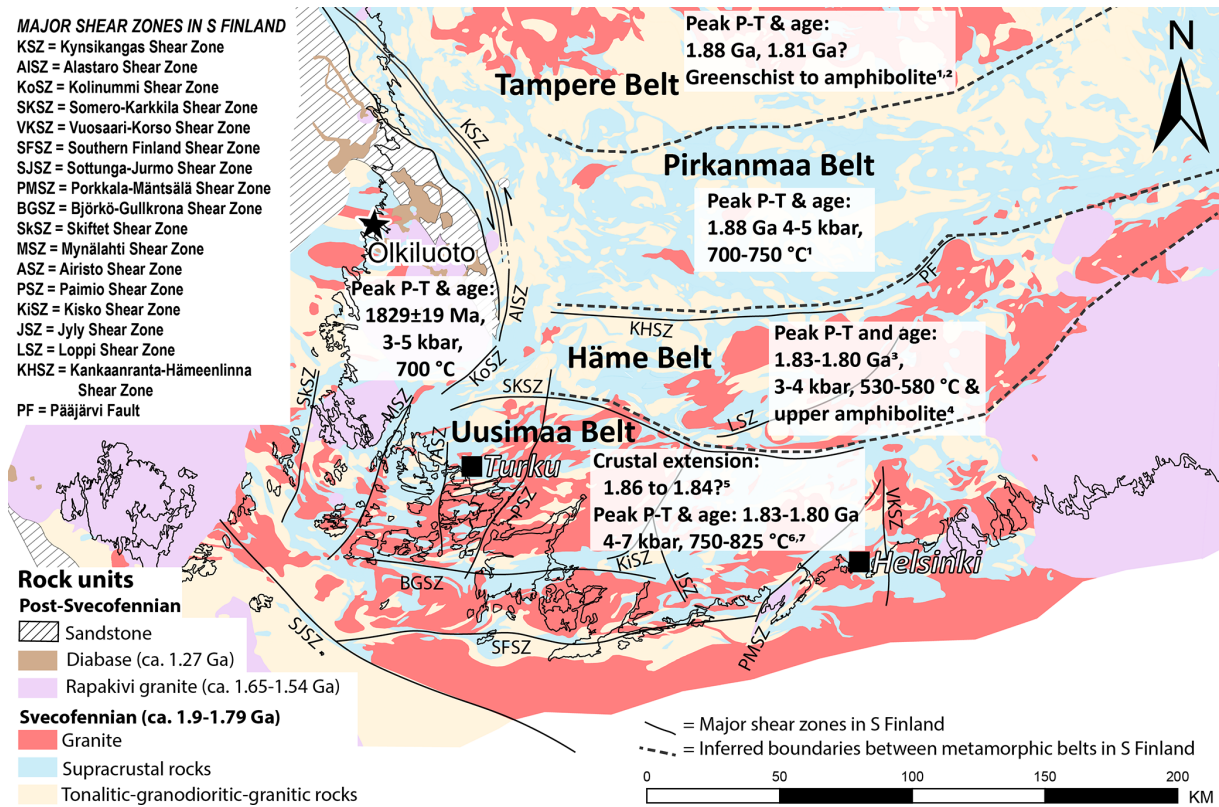
Figure 11. A geological map of southern Finland with the different tectonic and metamorphic belts and significant shear zones shown. The bedrock map scale is 1 : 200 000 and is taken from the Geological Survey of Finland (Geological Survey of Finland, 2022) (shear zones are adapted from Heeremans et al., 1996; Pitkälä et al., 2018; Reimers et al., 2018; Torvela et al., 2008; Torvela and Kurhila, 2022; Väisänen et al., 2014; Väisänen and Skyttä, 2007; and Lahtinen et al., 2023). The peak $P–T$ conditions and metamorphic ages are derived from the following references: (1) Mouri et al. (1999), (2) Lahtinen et al. (2017), (3) Hölttä et al. (2020), (4) Hölttä and Heilimo (2017), (5) Skyttä and Mänttäri (2008), (6) Mouri et al. (2005), and (7) Väisänen and Hölttä (1999).

pulses, as described by Chardon et al. (2009) for Precambrian accretionary orogens.

5.3 Implications for the tectonic framework of southern Finland

The tectonic framework for southern Finland possibly represents the distal regions in a back-arc basin complex that formed above the retreated subduction zone in the west and slab-rollback-caused (oblique) extension in the upper plate and asthenospheric upwelling in back-arc regions, following the proposed models (Collins, 2002; Hermansson et al., 2008; Saalmann et al., 2009; Kara et al., 2021). This caused high heat flow, decompression melting, and mafic underplating of the thinned continental crust, giving rise to melt production, intense magmatic activity, and granulite facies metamorphism in its deeper parts (Väisänen and Hölttä, 1999). This infers different crustal depths for the Häme Belt and Uusimaa Belt (Saalmann et al., 2009; Torvela and Kurhila, 2020). The presence of several shear zones in southern Finland is indicative of a transpressive tectonic regime that could be explained by strain partitioning in the oblique tectonic

regime where contractional segments were coupled to folding and thrusting, which is especially observed in the Häme Belt (Kara et al., 2021; Nironen, 1999; Pitkälä et al., 2018; Saalmann et al., 2009), whereas in the Uusimaa Belt the tectonic regime exhibits more transtensional shear zones (Väisänen and Skyttä, 2007; Torvela and Kurhila, 2022).

The Olkiluoto region is inferred to be coupled to the Häme Belt (see Sect. 5.2) with the Somero-Karkkila Shear Zone (SKSZ) acting as a metamorphic boundary between the Häme Belt and the Uusimaa Belt. However, the mosaic structure with shear zones and different crustal blocks that is characteristic for southern Finland shows that detailed comprehensive studies coupled with both structural geology and metamorphic studies are essential when determining the character and tectonic evolution of the crystalline bedrock in the high-grade environment that is prevailing in this tectonic domain. The impact of these crustal-scale shear zones in the tectonic framework of southern Finland is evident, but the kinematic constraints and age relationships are still poorly understood. However, most of these shear zones show ductile deformation signatures inferring deeper and hotter origins,

indicating formation before the ductile–brittle transition interpreted at ca. 1.78 Ga (Nordbäck et al., 2024).

5.4 Connection to Ljusdal lithotectonic unit

This study is an additional piece of the puzzle linking the crustal units of southwestern Finland and central Sweden. Only a limited number of studies are available, and clearly more studies are needed, especially in the Bothnian Basin separating Sweden and Finland to unravel, for example, if a failed rifting event is the cause of the separation and why sedimentary units are mainly present offshore (Korja and Heikkinen, 2005; Buntin et al., 2019; Fig. 1). Structural studies from southwestern Finland by Nordbäck et al. (2024) emphasize that large N–S structures are related to this rifting and to the development of the Mesoproterozoic sedimentary basin at the centre of Fennoscandian shield, which is located beneath the Bothnian Sea (e.g. Kohonen and Rämö, 2005). Thus, it is reasonable to assume that prior to this rifting event central Sweden and southwestern Finland were connected, as proposed by Engström et al. (2022) and by Luth et al. (2024) in the lithotectonic map of Fennoscandia. Further evidence is supported by the presence of similar mineralogy cordierite–sillimanite–garnet mineral assemblage in both Ljusdal and Olkiluoto (Högdahl and Bergman, 2020; Engström et al., 2022). The prolonged ductile deformation with several crustal-scale melt pulses indicates that the Olkiluoto site is similar to the Ljusdal lithotectonic unit in central Sweden (Högdahl et al., 2012; Engström et al., 2022; Fig. 1). Earlier studies by Engström et al. (2022) and Saukko et al. (2020) defined that the area was subjected to a high-grade migmatitic event during an approximate time span of 90 Ma between 1.87–1.78 Ga, with two main migmatite-producing events. Hence, it is plausible that the Häme Belt, including the Olkiluoto site, is connected to the Ljusdal lithotectonic unit. The major crustal-scale Kynsikangas shear zone located 40 km northeast of Olkiluoto possibly marks the tectonic boundary between the lithotectonic units (Fig. 11; Engström et al., 2022). The Saimaa orocline is deduced to be a big suture zone between the WFS and SFS in studies in eastern Finland (Lahtinen et al., 2022) and a likely continuation of that is the Kynsikangas shear zone, with a possible continuation to the Hassela shear zone in central Sweden (Reimers et al., 2018; Högdahl and Bergman, 2020; Lahtinen et al., 2023).

6 Conclusions

The previously published structural data (Engström et al., 2022), together with the metamorphic data presented in this paper, suggest that the Häme Belt, including the Olkiluoto area, and the Ljusdal lithotectonic unit share a similar deformation history and metamorphic $P–T–t$ conditions (Högdahl et al., 2008; Hölttä and Heilimo, 2017; Högdahl and

Bergman, 2020; Saukko et al., 2020; Lahtinen et al., 2023; Luth et al., 2024). Both areas show a younger ca. 1.83 Ga amphibolite facies metamorphic peak and possibly an older ca. 1.86 Ga metamorphic event.

The main outcome from this study are as follows.

- The garnets in the TGG type rock at the Olkiluoto site were studied, and in situ Lu–Hf geochronology defined a metamorphic peak at 1829 ± 19 Ma.

- The $P–T$ modelling at the site indicates peak $P–T$ conditions of 3–5 kbar and around 700 °C.

- The metamorphic evolution in southern Finland is poorly constrained due to complex structural geological evolution. This study provides valuable input to better constrain the metamorphic similarities between the Olkiluoto site and the Häme Belt. However, more metamorphic studies in both the Uusimaa Belt and the Häme Belt are needed to further constrain this.

- The Olkiluoto site is located between southern Finland and central Sweden and thus represents a key location to define a missing link between the Swedish and Finnish lithotectonic units. This study presents new results coupling these crustal units together.

Author contributions. JE: conceptualization, methodology, interpretation, visualization, writing (original draft). KC: conceptualization, methodology, interpretation, visualization, writing (review and editing). SG: in situ Lu–Hf geochronology, validation, writing (review). EH: whole-rock geochemistry, writing (review and editing). EMJ: micro-XRF analysis, writing (review). RMM: EPMA analysis, writing (review).

Disclaimer. Publisher's note: Copernicus Publications remains neutral with regard to jurisdictional claims made in the text, published maps, institutional affiliations, or any other geographical representation in this paper. While Copernicus Publications makes every effort to include appropriate place names, the final responsibility lies with the authors.

References

Aaltonen, I., Engström, J., Front, K., Gehör, S., Kosunen, P., Kärki, A., Mattila, J., Paananen, M., and Paulamäki, S.: Geology of Olkiluoto, Posiva Report 2016-16. Posiva Oy, Eurajoki, 404 pp., https://www.posiva.fi/en/index/media/reports.html (last access: 3 February 2025), 2016.

Bergman, S., Högdahl, K., Nironen, M., Ogenhall, E., Sjöström, H., Lundqvist, L., and Lahtinen, R.: Timing of Palaeoproterozoic intra-orogenic sedimentation in the central Fennoscandian Shield; evidence from detrital zircon in metasandstone, Precambrian Res., 161, 231–249, https://doi.org/10.1016/j.precamres.2007.08.007, 2008.

Brown, D. A., Simpson, A., Hand, M., Morrisey, L. J., Gilbert, S., Tamblyn, R., and Glorie, S.: Laser-ablation Lu–Hf dating reveals Laurentian garnet in subducted rocks from southern Australia, Geology, 50, 837–842, https://doi.org/10.1130/G49784.1, 2022.

Buntin, S., Malehmir, A., Koyi, H., Högdahl, K., Malinowski, M., Larsson, S. Å., Thybo, H., Juhlin, C., Korja, A., and Górszczyk, A.: Emplacement and 3D geometry of crustal-scale saucer-shaped intrusions in the Fennoscandian Shield, Nat. Sci. Rep., 9, 10498, https://doi.org/10.1038/s41598-019-46837-x, 2019.

Caddick, M. J., Konpoasek, J., and Thompson, A. B.: Preservation of Garnet Growth Zoning and the Duration of Prograde Metamorphism, J. Metamorph. Geol., 51, 2327–2347, https://doi.org/10.1093/petrology/egq059, 2010.

Chardon, D., Gapais, D., and Cagnard, F.: Flow of ultra-hot orogens: A view from the Precambrian, clues for the Phanerozoic, Tectonophysics, 477, 105–118, https://doi.org/10.1016/j.tecto.2009.03.008, 2009.

Chew, D. M. and Spikings, R. A.: Apatite U–Pb Thermochronology: A Review, Minerals, 11, 1095, https://doi.org/10.3390/min11101095, 2021.

Chew, D. M., Petrus, J. A., and Kamber, B. S.: U–Pb LA–ICPMS dating using accessory mineral standards with variable common Pb, Chem. Geol., 363, 185, https://doi.org/10.1016/j.chemgeo.2013.11.006, 2014.

Chopin, F., Korja, A., Nikkilä, K., Hölttä, P., Korja, T., Zaher, M. A., Kurhila, M., Eklund, O., and Rämö, O. T.: The Vaasa Migmatitic Complex (Svecofennian Orogen, Finland): Buildup of a LP-HT

Dome During Nuna Assembly, Tectonics, 39, e2019TC005583. https://doi.org/10.1029/2019TC005583, 2020.

Collins, W. J.: Hot orogens, tectonic switching, and creation of continental crust, Geology, 30, 535–538, https://doi.org/10.1130/0091-7613(2002)030<0535:HOTSAC>2.0.CO;2, 2002.

de Capitani, C. and Petrakakis, K.: The computation of equilibrium assemblage diagrams with Theriak/Domino software, Am. Mineral., 95, 1006–1016, https://doi.org/10.2138/am.2010.3354, 2010.

Ehlers, C., Lindroos, A., and Selonen, O.: The late Svecofennian granite-migmatite zone of southern Finland – a belt of transpressive deformation and granite emplacement, Precambrian Res., 64, 295–309, https://doi.org/10.1016/0301-9268(93)90083-E, 1993.

Engström, J., Kärki, A., Paulamäki, S., and Mänttäri, I.: Palaeoproterozoic structural evolution of polyphase migmatites in Olkiluoto, SW Finland, Bull. Geol. Soc. Finl., 94, 119–144, https://doi.org/10.17741/bgsf/94.2.002, 2022.

Engström, J., Cutts, K., Glorie, S., Heilimo, E., Jolis, E., and Michallik, R.: In situ Lu-Hf dating of garnet and apatite from Olkiluoto, southwestern Finland, EarthChem [data set], https://doi.org/10.60520/IEDA/113675, 2025.

Gaál, G. and Gorbatschev, R.: An Outline of the Precambrian Evolution of the Baltic Shield, Precambrian Res., 17, 149–159, https://doi.org/10.1016/0301-9268(87)90044-1, 1987.

Geological Survey of Finland: Geological bedrock map of Finland, https://hakku.gtk.fi/en (last access: 3 February 2025), 2022.

Gillespie, J., Glorie, S., Khudoley, A., and Collins, A.: Detrital apatite U–Pb and trace element analysis as a provenance tool: insights from the Yenisey Ridge (Siberia), Lithos, 314–315, 140–155, https://doi.org/10.1016/j.lithos.2018.05.026, 2018.

Glorie, S., Gillespie, J., Simpson, A., Gilbert, S., Khudoley, A., Priyatkina, N., Hand, M., and Kirkland, C. L.: Detrital apatite Lu–Hf and U–Pb geochronology applied to the southwestern Siberian margin, Terra Nova, 34, 201–209, https://doi.org/10.1111/ter.12580, 2022.

Glorie, S., Hand, M., Mulder, J., Simpson, A., Emo, R. B., Kamber, B., Fernie, N., Nixon, A., and Gilbert, S.: Robust laser ablation Lu–Hf dating of apatite: an empirical evaluation, Geol. Soc. Lond. Spec. Publ., 537, 165–184, https://doi.org/10.1144/SP537-2022-205, 2024a.

Glorie, S., Simpson, A., Gilbert, S. E., Hand, M., and Müller, A. B.: Testing the reproducibility of in situ Lu–Hf dating using Lu-rich garnet from the Tørdal pegmatites, southern Norway, Chem. Geol., 653, 122038, https://doi.org/10.1016/j.chemgeo.2024.122038, 2024b.

Glorie, S. M., Jepson, G., Konopelko, D., Mirkamalov, R., Meeuws, F., Gilbert, S., Gillespie, J., Collins, A., Xiao, W., Dewaele, S., and De Grave, J.: Thermochronological and geochemical footprints of post-orogenic fluid alteration recorded in apatite: implications for mineralisation in the Uzbek Tian Shan, Gondwana Res., 71, 1–15, https://doi.org/10.1016/j.gr.2019.01.011, 2019.

Heeremans, M., Stel, H., Van Der Beek, P., and Lankreijer, A.: Tectono-magmatic control on vertical dip slip basement faulting: An example from the Fennoscandian Shield, Terra Nova, 8, 129–140, https://doi.org/10.1111/j.1365-3121.1996.tb00737.x, 1996.

Heilimo, E., Mikkola, P., Ahven, M., Huhma, H., Lahaye, Y., and Virtanen, V. J.: Evidence of crustal growth dur-

ing the Svecofennian orogeny: New isotopic data from the central parts of the Paleoproterozoic Central Finland Granitoid Complex, Precambrian Res., 395, 107125, https://doi.org/10.1016/j.precamres.2023.107125, 2023.

Hermansson, T., Stephens, M. B., Corfu, F., Page, L. M., and Andersson, J.: Migratory tectonic switching, western Svecofennian orogen, central Sweden: Constraints from U/Pb zircon and titanite geochronology, Precambrian Res., 161, 250–278, https://doi.org/10.1016/j.precamres.2007.08.008, 2008.

Hietanen, A.: Generation of potassium-poor magmas in the northern Sierra Nevada and the Svecofennian in Finland, J. Res. US Geol. Surv., 1975, 631–645, 1975.

Högdahl, K. and Bergman, S.: Chapter 5 Paleoproterozoic (1.9–1.8 Ga), syn-orogenic magmatism and sedimentation in the Ljusdal lithotectonic unit, Svecokarelian orogen, Geol. Soc. Lond. Mem., 50, 131–153, https://doi.org/10.1144/M50-2016-30, 2020.

Högdahl, K., Majka, J., Sjöström, H., Nilsson, K. P., Claesson, S., and Koneèný, P.: Reactive monazite and robust zircon growth in diatexites and leucogranites from a hot, slowly cooled orogen: implications for the Palaeoproterozoic tectonic evolution of the central Fennoscandian Shield, Sweden, Contrib. Mineral. Petr. 163, 167–188, https://doi.org/10.1007/s00410-011-0664-x, 2012.

Högdahl, K., Sjöström, H., Andersson, U. B., and Ahl, M.: Continental margin magmatism and migmatisation in the west-central Fennoscandian Shield, Lithos, 102, 435–459, https://doi.org/10.1016/j.lithos.2007.07.019, 2008.

Holland, T. and Powell, R.: Activity–composition relations for phases in petrological calculations: an asymmetric multicomponent formulation, Contrib. Mineral. Petrol., 145, 492–501, https://doi.org/10.1007/s00410-003-0464-z, 2003.

Holland, T. J. B. and Powell, R.: An improved and extended internally consistent thermodynamic dataset for phases of petrological interest, involving a new equation of state for solids, J. Metamorph. Geol., 29, 333–383, https://doi.org/10.1111/j.1525-1314.2010.00923.x, 2011.

Hölttä, P. and Heilimo, E.: Metamorphic Map of Finland, Spec. Pap.-Geol. Surv. Finl., 60, 75–126, 2017.

Hölttä, P., Huhma, H., Lahaye, Y., Mänttäri, I., Lukkari, S., and O'Brien, H.: Paleoproterozoic metamorphism in the northern Fennoscandian Shield: age constraints revealed by monazite, Int. Geol. Rev., 62, 360–387, https://doi.org/10.1080/00206814.2019.1611488, 2020.

Irvine, T. N. and Baragar, W. R. A.: A Guide to the Chemical Classification of the Common Volcanic Rocks, Can. J. Earth Sci., 8, 523–548, https://doi.org/10.1139/e71-055, 1971.

Jørgensen, T. R. C., Tinkham, D. K., and Lesher, C. M.: Low-P and high-T metamorphism of basalts: Insights from the Sudbury impact melt sheet aureole and thermodynamic modelling, J. Metamorph. Geol., 37, 271–313, https://doi.org/10.1111/jmg.12460, 2019.

Kähkönen, Y.: Chapter 8 Svecofennian supracrustal rocks, in: Developments in Precambrian Geology, Precambrian Geology of Finland Key to the Evolution of the Fennoscandian Shield, edited by: Lehtinen, M., Nurmi, P. A., and Rämö, O. T., Elsevier, 343–405, https://doi.org/10.1016/S0166-2635(05)80009-X, 2005.

Kara, J., Leskelä, T., Väisänen, M., Skyttä, P., Lahaye, Y., Tiainen, M., and Leväniemi, H.: Early Svecofennian rift-related magmatism: Geochemistry, U–Pb–Hf zircon isotope data and tectonic setting of the Au-hosting Uunimäki gabbro, SW Finland, Precambrian Res., 364, 106364, https://doi.org/10.1016/j.precamres.2021.106364, 2021.

Kärki, A.: Migmatites and Migmatite-Like Rocks of Olkiluoto, Working Report No. 2015–03, Posiva Working Report, Posiva Oy, Eurajoki, https://www.posiva.fi/en/index/media/reports.html (last access: 3 February 2025), 2015.

Kärki, A. and Paulamäki, S.: Petrology of Olkiluoto, Posiva Report No. 2006–02, Posiva Oy, Olkiluoto, https://www.posiva.fi/en/index/media/reports.html (last access: 3 February 2025), 2006.

Kohonen, J. and Rämö, O. T.: Chapter 13 Sedimentary rocks, diabases, and late cratonic evolution, in: Developments in Precambrian Geology, Precambrian Geology of Finland Key to the Evolution of the Fennoscandian Shield, edited by: Lehtinen, M., Nurmi, P. A., and Rämö, O. T., Elsevier, 563–603, https://doi.org/10.1016/S0166-2635(05)80014-3, 2005.

Kohonen, J., Lahtinen, R., Luukas, J., and Nironen, M.: Classification of regional-scale tectonic map units in Finland, Geol. Surv. Finl. Bull., 33–80, https://doi.org/10.30440/bt412.2, 2021.

Koistinen, T., Bogatchev, V., Stephens, M. B., Nordgulen, O., Wennerström, M., and Korhonen, J.: Geological map of the Fennoscandian Shield scale 1 : 2 000 000, Geological Survey of Finland, Trond-heim: Geological Survey of Norway, Uppsala: GeologicalSurvey of Sweden, Moscow: Ministry of Natural Resources of Russia, https://hakku.gtk.fi/en (last access: 3 February 2025), 2001.

Korja, A. and Heikkinen, P.: The accretionary Svecofennian orogen – insight from the BABEL profiles, Precambrian Res., 136, 241–268, https://doi.org/10.1016/j.precamres.2004.10.007, 2005.

Korsman, K., Koistinen, T., Kohonen, J., Wennerström, M., Ekdahl, E., Honkamo, M., and Idman, H.: Suomen kallioperäkartta = Berggrundskarta över Finland = Bedrock map of Finland, https://hakku.gtk.fi/en (last access: 3 February 2025), 1997.

Korsman, K., Korja, T., Pajunen, M., Virransalo, P., and GGT/SVEKA Working Group: The GGT/SVEKA Transect: Structure and Evolution of the Continental Crust in the Paleoproterozoic Svecofennian Orogen in Finland, Int. Geol. Rev., 41, 287–333, https://doi.org/10.1080/00206819909465144, 1999.

Kurhila, M., Mänttäri, I., Vaasjoki, M., Tapani Rämö, O., and Nironen, M.: U–Pb geochronological constraints of the late Svecofennian leucogranites of southern Finland, Precambrian Res., 190, 1–24, https://doi.org/10.1016/j.precamres.2011.07.008, 2011.

Lahtinen, R., Korja, A., and Nironen, M.: Precambrian Geology of Finland Key to the Evolution of the Fennoscandian Shield, in: Developments in Precambrian Geology, Paleoproterozoic tectonic evolution, Chap. 11, Elsevier, https://doi.org/10.1016/S0166-2635(05)80012-X, 2005.

Lahtinen, R., Huhma, H., Sipilä, P., and Vaarma, M.: Geochemistry, U–Pb geochronology and Sm–Nd data from the Paleoproterozoic Western Finland supersuite – A key component in the coupled Bothnian oroclines, Precambrian Res., 299, 264–281, https://doi.org/10.1016/j.precamres.2017.07.025, 2017.

Lahtinen, R., Salminen, P. E., Sayab, M., Huhma, H., Kurhila, M., and Johnston, S. T.: Age and structural constraints on the tectonic evolution of the Paleoproterozoic Saimaa orocline in Fennoscandia, Precambrian Res., 369, 106477, https://doi.org/10.1016/j.precamres.2021.106477, 2022.

Lahtinen, R., Köykkä, J., Salminen, J., Sayab, M., and Johnston, S. T.: Paleoproterozoic tectonics of Fennoscandia and the birth of Baltica, Earth-Sci. Rev., 246, 104586, https://doi.org/10.1016/j.earscirev.2023.104586, 2023.

Lanari, P., Vidal, O., De Andrade, V., Dubacq, B., Lewin, E., Grosch, E. G., and Schwartz, S.: XMapTools: A MATLAB©-based program for electron microprobe X-ray image processing and geothermobarometry, Comput. Geosci., 62, 227–240, https://doi.org/10.1016/j.cageo.2013.08.010, 2014.

Lane, K. M.: Metamorphic and geochronological constraints on the evolution of the Kalinjala Shear Zone, Eyre Peninsula, PhD thesis, University of Adelaide, http://hdl.handle.net/2440/96684 (last access: 3 February 2025), 2011.

Li, Y. and Vermeesch, P.: Short communication: Inverse isochron regression for Re–Os, K–Ca and other chronometers, Geochronology, 3, 415–420, https://doi.org/10.5194/gchron-3-415-2021, 2021.

Luth, S., Torgersen, E., and Köykkä, J.: Lithotectonic map of Fennoscandia, in: 36th Nordic Geological Winter Meeting, Göteborg, edited by: Regnéll, C., Zack, T., Holme, K., and Andersson, J., Nordic Gelogical Winter Meeting 2024, Gothenburg, 10–12 January 2024, 558 pp., ISBN 978-91-987833-4-6 https://geologiskaforeningen.se/wp-content/uploads/2024/04/GF_SP5_2024_abstract-volume.pdf (last access: 3 February 2025), 2024.

Mäkitie, H., Sipilä, P., Kujala, H., Lindberg, A., and Kotilainen, A.: Formation mechanism of the Vaasa Batholith in the Fennoscandian shield: Petrographic and geochemical constraints, Bull. Geol. Soc. Finl., 84, 141–166, https://doi.org/10.17741/bgsf/84.2.003, 2012.

Mänttäri, I., Talikka, M., Paulamäki, S., and Mattila, J.: U–Pb ages for tonalitic gneiss, pegmatitic granite, and diabase dyke, Olkiluoto study site, Eurajoki, SW Finland, Working Report No. 2006–12, Posiva Working Report, Posiva Oy, Eurajoki, https://www.posiva.fi/en/index/media/reports.html (last access: 3 February 2025), 2006.

Mark, C., O'Sullivan, G., Glorie, S., Simpson, A., Andò, S., Barbarano, M., Stutenbecker, L., Daly, J. S., and Gilbert, S.: Detrital Garnet Geochronology by In Situ U–Pb and Lu–Hf Analysis: A Case Study From the European Alps, J. Geophys. Res.-Earth, 128, e2023JF007244, https://doi.org/10.1029/2023JF007244, 2023.

McDonough, W. F. and Sun, S.: The composition of the Earth, Chem. Geol., 120, 223–253, https://doi.org/10.1016/0009-2541(94)00140-4, 1995.

Middlemost, E. A. K.: Naming materials in the magma/igneous rock system, Earth-Sci. Rev., 37, 215–224, https://doi.org/10.1016/0012-8252(94)90029-9, 1994.

Mouri, H., Korsman, K., and Huhma, H.: Tectono-metamorphic evolution and timing of the melting processes in the Svecofennian Tonalite-Trondhjemite Migmatite Belt: An example from Luopioinen, Tampere area, southern Finland, Bull. Geol. Soc. Finl., 71, 31–56, https://doi.org/10.17741/bgsf/71.1.003, 1999.

Mouri, H., Väisänen, M., Huhma, H., and Korsman, K.: Sm–Nd garnet and U–Pb monazite dating of high-grade metamorphism and crustal melting in the West Uusimaa area, southern Finland, GFF, 127, 123–128, https://doi.org/10.1080/11035890501272123, 2005.

Nebel, O., Morel, M., and Vroon, P.: Isotope Dilution Determinations of Lu, Hf, Zr, Ta and W, and Hf Isotope Compositions of NIST SRM 610 and 612 Glass Wafers, Geostand. Geoanal. Res., 33, 487–499, 2009.

Nironen, M.: The Svecofennian Orogen: A tectonic model, Precambrian Res., 86, 21–44, https://doi.org/10.1016/S0301-9268(97)00039-9, 1997.

Nironen, M.: Structural and magmatic evolution in the Loimaa area, southwestern Finland, Bull. Geol. Soc. Finl., 71, 57–71, https://doi.org/10.17741/bgsf/71.1.004, 1999.

Nironen, M.: Chapter 10 Proterozoic orogenic granitoid rocks, in: Developments in Precambrian Geology, Precambrian Geology of Finland Key to the Evolution of the Fennoscandian Shield, edited by: Lehtinen, M., Nurmi, P. A., and Rämö, O. T., Elsevier, 443–479, https://doi.org/10.1016/S0166-2635(05)80011-8, 2005.

Nironen, M.: Bedrock of Finland at the scale 1 : 1 000 000 – Major stratigraphic units, metamorphism and tectonic evolution, Geological Survey of Finland, Special Paper 60, ISBN 978-952-217-380-5, https://minsysfin.gtk.fi/wp-content/uploads/sp_060.pdf (last access: 3 February 2025), 2017.

Nordbäck, N., Mattila, J., Zwingmann, H., and Viola, G.: Precambrian fault reactivation revealed by structural and K–Ar geochronological data from the spent nuclear fuel repository in Olkiluoto, southwestern Finland, Tectonophysics, 824, 229208, https://doi.org/10.1016/j.tecto.2022.229208, 2022.

Nordbäck, N., Skyttä, P., Engström, J., Ovaskainen, N., Mattila, J., and Aaltonen, I.: Mesoproterozoic Strike-Slip Faulting within the Åland Rapakivi Batholith, Southwestern Finland, Tektonika, 2, 1–26, https://doi.org/10.55575/tektonika2024.2.1.51, 2024.

Norris, A. and Danyushevsky, L.: Towards estimating the complete uncertainty budget of quantified results measured by LA-ICP-MS, Goldschmidt, Boston, USA, Poster 195 in session 06j, 16–17 August 2018, https://goldschmidtabstracts.info/abstracts/abstractView?id=2018003403 (last access: 3 February 2025), 2018.

O'Sullivan, G., Chew, D., Kenny, G., Henrichs, I., and Mulligan, D.: The trace element composition of apatite and its application to detrital provenance studies, Earth-Sci. Rev. 201, 103044, https://doi.org/10.1016/j.earscirev.2019.103044, 2020.

Pitkälä, I., Kara, J., Leskelä, T., Skyttä, P., Väisänen, M., Leväniemi, H., Hokka, J., Tiainen, M., and Lahaye, Y.: Shear zones and structural analysis of the Loimaa area, SW Finland, in: Lithosphere 2018 – Tenth Symposium on the Structure, Composition and Evolution of the Lithosphere in Fennoscandia, Programme and extended Abstracts, Institute of Seismology University of Helsinki report S-67, https://www.seismo.helsinki.fi/ilp/lito2018/Lito2018_Abstract_Volume_color.pdf (last access: 3 February 2025), 2018.

Pouchou, J. L. and Pichoir, F.: Basic expression of "PAP" computation for quantitative EPMA, in: 11th International Congress on X – Ray Optics and Microanalysis (ICXOM), London Canada, 4–8 August 1986, edited by: Brown, J. D. and Packwood, R. H., 249–253, https://search.worldcat.org/title/222411343 (last access: 3 February 2025), 1986.

Reimers, S., Engström, J., and Riller, U.: The Kynsikangas shear zone, Southwest Finland: Importance for understanding deformation kinematics and rheology of lower crustal shear zones, in: Lithosphere 2018 – Tenth Symposium on the Structure, Composition and Evolution of the Lithosphere in Fennoscandia, Pro-

gramme and extended Abstracts, Institute of Seismology University of Helsinki Report S-67, https://www.seismo.helsinki.fi/ilp/lito2018/Lito2018_Abstract_Volume_color.pdf (last access: 3 February 2025), 2018.

Saalmann, K., Mänttäri, I., Ruffet, G., and Whitehouse, M. J.: Age and tectonic framework of structurally controlled Palaeoproterozoic gold mineralization in the Häme belt of southern Finland, Precambrian Res., 174, 53–77, https://doi.org/10.1016/j.precamres.2009.06.005, 2009.

Saalmann, K., MäNttäRi, I., Peltonen, P., Whitehouse, M. J., GröNholm, P., and Talikka, M.: Geochronology and structural relationships of mesothermal gold mineralization in the Palaeoproterozoic Jokisivu prospect, southern Finland, Geol. Mag., 147, 551–569, https://doi.org/10.1017/S0016756809990628, 2010.

Saukko, A., Ahläng, C., Nikkilä, K., Soesoo, A., and Eklund, O.: Double Power-Law in Leucosome Width Distribution: Implications for Recognizing Melt Movement in Migmatites, Front. Earth Sci., 8, 591871, https://doi.org/10.3389/feart.2020.591871, 2020.

Simpson, A., Gilbert, S., Tamblyn, R., Hand, M., Spandler, C., Gillespie, J., Nixon, A., and Glorie, S.: In-situ LuHf geochronology of garnet, apatite and xenotime by LA ICP MS/MS, Chem. Geol., 577, 120299, https://doi.org/10.1016/j.chemgeo.2021.120299, 2021.

Simpson, A., Glorie, S., Hand, M., Spandler, C., and Gilbert, S.: Garnet Lu–Hf speed dating: A novel method to rapidly resolve polymetamorphic histories, Gondwana Res., 121, 215–234, https://doi.org/10.1016/j.gr.2023.04.011, 2023.

Skyttä, P. and Mänttäri, I.: Structural setting of late Svecofennian granites and pegmatites in Uusimaa Belt, SW Finland: Age constraints and implications for crustal evolution, Precambrian Res., 164, 86–109, https://doi.org/10.1016/j.precamres.2008.04.001, 2008.

Smit, M. A., Vrijmoed, J. C., Scherer, E. E., Mezger, K., Kooijman, E., Schmitt-Kielman, M., Tual, L., Guilmette, C., and Ratschbacher, L.: Retentiveness of rare earth elements in garnet with implications for garnet Lu–Hf chronology, J. Metamorph. Geol., 42, 1–25, https://doi.org/10.1111/jmg.12769, 2024.

Söderlund, U., Patchett, P. J., Vervoort, J. D., and Isachsen, C. E.: The ^{176}Lu decay constant determined by Lu–Hf and U–Pb isotope systematics of Precambrian mafic intrusions, Earth Planet. Sc. Lett., 219, 311–324, https://doi.org/10.1016/S0012-821X(04)00012-3, 2004.

Spencer, C. J., Kirkland, C. L., Roberts, N. M. W., Evans, N. J., and Liebmann, J.: Strategies towards robust interpretations of in situ zircon Lu–Hf isotope analyses, Geosci. Front., 11, 843–853, https://doi.org/10.1016/j.gsf.2019.09.004, 2020.

Stephens, M. B.: Chapter 1 Introduction to the lithotectonic framework of Sweden and organization of this Memoir, Geol. Soc. Lond. Mem., 50, 1–15, https://doi.org/10.1144/M50-2019-21, 2020.

Tamblyn, R., Hand, M., Simpson, A., Gilbert, S., Wade, B., and Glorie, S.: In situ laser ablation Lu–Hf geochronology of garnet across the Western Gneiss Region: campaign-style dating of metamorphism, J. Geol. Soc., 179, jgs2021-094, https://doi.org/10.1144/jgs2021-094, 2022.

Thompson, J., Meffre, S., Maas, R., Kamenetsky, V., Kamenetsky, M., Goemann, K., Ehrig, K., and Danyushevsky, L.: Matrix effects in Pb/U measurements during LA-ICP-MS analysis of the mineral apatite, J. Anal. Atom. Spectrom., 31, 1206–1215, https://doi.org/10.1039/C6JA00048G, 2016.

Thomson, S. N., Gehrels, G. E., Ruiz, J., and Buchwaldt, R.: Routine low-damage apatite U–Pb dating using laser ablation–multicollector–ICPMS, Geochem. Geophy. Geosy., 13, Q0AA21, https://doi.org/10.1029/2011GC003928, 2012.

Torvela, T. and Kurhila, M.: How does orogenic crust deform? Evidence of crustal-scale competent behaviour within the partially molten middle crust during orogenic compression, Precambrian Res., 342, 105670, https://doi.org/10.1016/j.precamres.2020.105670, 2020.

Torvela, T. and Kurhila, M.: Timing of syn-orogenic, high-grade transtensional shear zone formation in the West Uusimaa Complex, Finland, Bull. Geol. Soc. Finl., 18, 5–22, https://doi.org/10.17741/bgsf/94.1.001, 2022.

Torvela, T., Mänttäri, I., and Hermansson, T.: Timing of deformation phases within the South Finland shear zone, SW Finland, Precambrian Res., 160, 277–298, https://doi.org/10.1016/j.precamres.2007.08.002, 2008.

Tuisku, P. and Kärki, A.: Metamorphic Petrology of Olkiluoto, Working Report No. 2010–54, Posiva Working Report. Posiva Oy, Eurajoki, https://www.posiva.fi/en/index/media/reports.html (last access: 3 February 2025), 2010.

Väisänen, M. and Hölttä, P.: Structural and metamorphic evolution of the Turku migmatite complex, southwestern Finland, Bull. Geol. Soc. Finl., 71, 177–218, https://doi.org/10.17741/bgsf/71.1.009, 1999.

Väisänen, M. and Skyttä, P.: Late Svecofennian shear zones in southwestern Finland, GFF, 129, 55–64, https://doi.org/10.1080/11035890701291055, 2007

Väisänen, M., Mänttäri, I., and Hölttä, P.: Svecofennian magmatic and metamorphic evolution in southwestern Finland as revealed by U–Pb zircon SIMS geochronology, Precambrian Res., 116, 111–127, https://doi.org/10.1016/S0301-9268(02)00019-0, 2002.

Väisänen, M., Eklund, O., Lahaye, Y., O'Brien, H., Fröjdö, S., Högdahl, K., and Lammi, M.: Intra-orogenic Svecofennian magmatism in SW Finland constrained by LA-MC-ICP-MS zircon dating and geochemistry, GFF, 134, 99–114, https://doi.org/10.1080/11035897.2012.680606, 2012.

Väisänen, M., Simelius, C., O'Brien, H., Kyllästinen, M., and Mattila, J.: Late Svecofennian mafic magmatism in southern Finland, in: Eighth Symposium on Structure, Composition and Evolution of the Lithosphere in Fennoscandia Programme and extended Abstracts, p. 107, https://www.seismo.helsinki.fi/pdf/Lito2014.pdf (last access: 3 February 2025), 2014.

Vermeesch, P.: IsoplotR: A free and open toolbox for geochronology, Geosci. Front, 9, 1479–1493, https://doi.org/10.1016/j.gsf.2018.04.001, 2018

White, R. W., Powell, R., Holland, T. J. B., Johnson, T. E., and Green, E. C. R.: New mineral activity–composition relations for thermodynamic calculations in metapelitic systems, J. Metamorph. Geol., 32, 261–286, https://doi.org/10.1111/jmg.12071, 2014a.

White, R. W., Powell, R., and Johnson, T. E.: The effect of Mn on mineral stability in metapelites revisited: new a–x relations for manganese-bearing minerals, J. Metamorph. Geol., 32, 809–828, https://doi.org/10.1111/jmg.12095, 2014b.